Published OnlineFirst November 30, 2010; DOI:10.1158/0008-5472.CAN-10-1055

Cancer Research

Novel Metastasis-Related Gene CIM Functions in the Regulation of Multiple Cellular Stress–Response Pathways

Kiyoshi Yanagisawa[1,2], Hiroyuki Konishi[3], Chinatsu Arima[1], Shuta Tomida[1], Toshiyuki Takeuchi[1], Yukako Shimada[1], Yasushi Yatabe[4], Tetsuya Mitsudomi[5], Hirotaka Osada[3], and Takashi Takahashi[1]

Abstract

Various stresses of the tumor microenvironment produced by insufficient nutrients, pH, and oxygen can contribute to the generation of altered metabolic and proliferative states that promote the survival of metastatic cells. Among many cellular stress–response pathways activated under such conditions are the hypoxia-inducible factor (HIF) pathway and the unfolded protein response (UPR), which is elicited as a response to endoplasmic reticulum (ER) stress. In this study, we report the identification of a novel cancer invasion and metastasis-related gene (hereafter referred to as *CIM*, also called *ERLEC1*), which influences both of these stress–response pathways to promote metastasis. *CIM* was identified by comparing the gene expression profile of a highly metastatic human lung cancer cell line with its weakly metastatic parental clone. We showed that CIM is critical for metastatic properties in this system. Proteomic approaches combined with bioinformatic analyses revealed that CIM has multifaceted roles in controlling the response to hypoxia and ER stress. Specifically, CIM sequestered OS-9 from the HIF-1α complex and PHD2, permitting HIF-1α accumulation by preventing its degradation. Ectopic expression of CIM in lung cancer cells increased their tolerance to hypoxia. CIM also modulated UPR through interaction with the key ER stress protein BiP, influencing cell proliferation under ER stress conditions. Our findings shed light on how tolerance to multiple cellular stresses at a metastatic site can be evoked by an integrated mechanism involving CIM, which can function to coordinate those responses in a manner that promotes metastatic cell survival. *Cancer Res; 70(23); 9949–58. ©2010 AACR.*

Introduction

Lung cancer is the number 1 cause of cancer death in many economically developed countries including Japan, claiming an unacceptably large number of lives each year. Despite recent aggressive treatment approaches, and great strides in understanding its biology and the underlying molecular mechanisms (1), long-term survival rates remain unsatisfactory, with more than 50% of cases eventually suffering from widespread metastases or local recurrences after successful potentially curative resection (2). Although cancer metastasis has been considered to arise from a minute fraction of primary cancer cells through multistep clonal evolutions, accumulating evidence points to the possibility that metastatic potential is acquired early in carcinogenesis, consequently conferring metastatic capabilities to the bulk of primary tumors (3, 4). It is evidently an urgent need to elucidate how lung cancer cells give rise to distant metastasis to provide not only a better understanding of the underlying molecular mechanisms, but also reveal novel targets for greatly improved molecular diagnosis and therapeutic intervention.

Along this line, various investigators have shown that microarray analysis is a useful means to identify genes related to a metastatic phenotype (3, 5–7). We have established a highly metastatic clone (NCI-H460-LNM35, hereafter referred to as LNM35) of a non-small cell lung cancer cell line, which helped us to identify the involvement of the *COX-2*, *CLCP-1*, and *DLX-4* genes in lung cancer metastasis through microarray analyses (8–13). In addition, proteomics-based approaches, which are increasingly being used to gain insight into the molecular complexities of human cancers (14–17), have also been noted to be powerful in such studies (18–20).

Emerging evidence suggests that various types of cellular stress from the insufficient microenvironment surrounding metastatic cells, such as restriction of nutrients, pH changes, and oxygenation are important contributing elements that induce an altered metabolic and proliferative status, which favors their survival in metastatic sites (21, 22). Such microenvironment stresses activate a range of cellular stress–

Authors' Affiliations: [1]Division of Molecular Carcinogenesis, Center for Neurological Diseases and Cancer, Nagoya University Graduate School of Medicine, [2]Institute for Advanced Research, Nagoya University, [3]Division of Molecular Oncology, Aichi Cancer Center Research Institute, [4]Department of Pathology and Molecular Diagnostics, and [5]Department of Thoracic Surgery, Aichi Cancer Center Hospital, Nagoya, Japan

Corresponding Author: Takashi Takahashi, Nagoya University Graduate School of Medicine, 65 Tsurumai-cho, Showa-ku, Nagoya 466-8550, Japan. Phone: 81-52-744-2454; Fax: 81-52-744-2457; E-mail: tak@med.nagoya-u.ac.jp or Kiyoshi Yanagisawa, Division of Molecular Carcinogenesis, Center for Neurological Diseases and Cancer, Nagoya University Graduate School of Medicine, Nagoya 466-8550, Japan. Phone: 81-52-744-2454; Fax: 81-52-744-2457; E-mail: kyana@med.nagoya-u.ac.jp.

doi: 10.1158/0008-5472.CAN-10-1055

Published OnlineFirst November 30, 2010; DOI:10.1158/0008-5472.CAN-10-1055

response pathways, including those mediated by the hypoxia inducible factor (HIF) family of transcription factors as well as unfolded protein response (UPR; refs. 21–24). HIF-1 is a transcription factor that transactivates target genes involved in survival, proliferation, angiogenesis, invasion, and metastasis (25). HIF-1 is negatively regulated by von Hippel–Lindau (VHL) tumor suppressor-mediated ubiquitination, which also involves OS-9 and prolyl hydroxylases (26–29). UPR is a program of transcriptional and translational changes elicited as a response to endoplasmic reticulum (ER) stress and regulates the balance between survival and apoptosis, as well as between dormancy and aggressive growth of tumor cells (21, 22, 24). However, little is known regarding the underlying mechanisms that perturb this balance, which contributes to tumor progression such as establishment of cancer metastasis.

In the present study, we identified a gene associated with various characteristics of a highly metastatic NCI-H460-LNM35 human lung cancer cell line and characterized it in detail in relation to cancer metastasis through a combined omics approach that utilized microarray and mass spectrometry with peptide tagging technology followed by bioinformatic analyses. Our findings suggest that CIM has multifaceted roles in cancer metastasis, by positively regulating HIF-1α expression as well as by modulating cytoprotective UPR.

Materials and Methods

Cell lines, lung cancer tissues, RNA extraction, and MTT assay

NCI-H460 and 293T cell lines were used within 6 months of purchase from ATCC and maintained in Roswell Park Memorial Institute (RPMI) and DMEM with 10% fetal calf serum (FCS), respectively. ATCC provides molecular authentication in support of their collection. Establishment of NCI-H460-LNM35, a highly metastatic human lung cancer subline, and NCI-H460-N15, a low metastatic parental subline, has been reported previously (13), and these cell lines were cultured in RPMI with 10% FCS. In our hypoxia culture, cells were placed in a multigas incubator (Sanyo) with 0.5% O_2/5% CO_2/balance N_2 and incubated at 37°C. Tumor and normal lung tissues were collected from patients diagnosed histologically as primary lung cancer, who underwent potentially curative resection at Aichi Cancer Center Hospital between January 1996 and January 1998 (3 SCLC, 6 adenocarcinoma, 6 squamous cell carcinoma, and 1 large cell carcinoma cases). Approval from the institutional review board and the patients' written informed consent were obtained. Staging was determined after pathologic evaluation of resected specimens according to the International System for Staging Lung Cancer. All tissues were quickly frozen in liquid nitrogen and stored at −80°C until analysis. RNA was isolated using RNAeasy (Qiagen) according to the manufacturer's instructions, and the quality was checked with 2100 Bioanalyzer (Agilent). 3-(4,5-Dimethylthiazol-2-yl) 2,5 diphenyltetrazolium bromide (MTT) assay was performed with TetraColor One according to manufacturer's instruction (Seikagaku), and triplicate independent experimental repeats were performed and the data analyzed all together.

Microarray and Northern blot analyses

A cDNA membrane microarray (GeneFilter Human Microarrays GF202; Invitrogen,), containing a total of 5392 spots corresponding to 5184 unique genes was used to analyze a set of total RNA extracted from LNM35 and N15 cells (5 μg each; ref. 8). We conducted 2 independent experiments, and the results from each were analyzed separately. Raw expression data for each gene were normalized within each of the hybridization results (for LNM35) using a global normalization method. The expression values of LNM35 were compared to those of N15, and array spots that met the following criteria were selected; differential expression at the level of more than 3-fold elevation or reduction in LNM35 cells in both of 2 independent experiments. Northern blot analysis using 10 μg each of the extracted total RNA samples were conducted using standard procedures.

Generation of CIM knocked down LNM35 cells by transfecting CIM-specific shRNA expression vector

A CIM-specific shRNA expression vector and control vector were constructed by cloning annealed oligonucleotides of CIM-specific shRNA into pH1-RNAneo, in which gene expression is under the control of the RNA polymerase III H1-RNA gene promoter. LNM35 CIM-specific shRNA stable transfectants (clones #5–11, #6–4, #6–11, and #6–12) were generated by transfection of 2 μg of pH1-RNAneo-CIM-specific shRNA using FuGENE 6 reagent (Roche Applied Science). Cells were selected by the neomycin (1 mg/mL) for 2 weeks.

In vivo spontaneous metastasis assay

Cells (1.0×10^7) in 0.1 mL of serum-free RPMI 1640 medium were injected into the subcutaneous tissue of the right abdominal wall of six 6-week-old female SCID mice (CLEA Japan), which were maintained under specific-pathogen-free conditions. Forty days after inoculation, the mice were euthanized and their lungs, lymph nodes, and subcutaneous tumors were resected, weighed, and fixed with 4% formaldehyde. Lung-metastatic nodules were examined under a dissecting microscope. All the results presented were obtained by averaging these data. Animal care was in accord with institution guidelines.

Construction of the myc-tagged CIM expression vector and antibodies

Full-length *CIM* cDNA was generated by PCR using cDNA converted from normal lung RNA. The resultant PCR products were cloned into the pIRES-puro2-myc (Invitrogen) and sequenced thoroughly. To construct 2 expression vectors for an artificial truncation mutant that lacked the N- or C-terminal homologous region (HR) of OS-9, a myc-tagged CIM vector was constructed from pIRES-puro2-CIM-myc after digestion with BsrGI or EcoNI, respectively.

Antibodies, anti-myc, GRP75 and -LGALS3 (anti-myc for CIM detection, Santa Cruz Biotechnology), -HIF-1α and BiP (BD BioSciences), -OS-9 and -PHD2 (Novus), -KDEL, -GM130,

Published OnlineFirst November 30, 2010; DOI:10.1158/0008-5472.CAN-10-1055

caspase3, caspase8, PARP, IRE-1α, p38, and ERK (Cell Signaling) were used in this study.

Proteomic analysis

Cells were lysed with 100 μL of 0.5 mol/L TEAB containing 0.1% (w/v) SDS, as described previously (20), and centrifuged at 18,000 × *g* for 20 minutes at 4°C. One hundred micrograms of protein in the supernatants were labeled with iTRAQ (Applied Biosystems) according to the manufacturer's instructions. Peptide fractionation was performed using nano-HPLC (KYA Technologies) with trap, and strong cation exchange and reverse-phase (RP) analytical columns. The RP column eluate was analyzed using mass spectrometry (Q-STAR-XL; Applied Biosystems) and relative abundance of each protein was determined by the MS/MS scans of iTRAQ-labeled peptides. Proteins with more than 2-fold difference between VC and shCIM cells were analyzed further as candidate targets of CIM.

Gene ontology (GO; ref. 30) analysis was employed to highlight the functionally distinct biological features of a protein set associated with the acquisition of invasive and metastatic capabilities promoted by CIM in lung cancer cells, as described previously (8, 10). Proteins affected by the change in CIM expression were linked to GO terms using Gene Spring (Agilent), and then were subjected to Fisher's exact test to identify which GO terms were over- or under-represented in a protein set of interest. Network analysis was conducted using the interrelation search mode of the KeyMolnet software (Medicinal Molecular Design) under the 2 "path limit" condition.

Immunoprecipitation

293T cells (3×10^6) were transfected with 10 μg of myc-tagged CIM expression vectors. After 24 hours, the cells were lysed with PBS/0.1% Tween-20 and 500 μg of WCL was used for immunoprecipitation with an agarose conjugated anti-myc antibody (Santa Cruz Biotechnology).

Analysis of XBP-1 splicing

First-strand cDNA was synthesized using SuperScript (Invitrogen). cDNAs were amplified with the 5′-AAGACAGCGCTTGGGGATGG-3′ and 5′-TCCATGGGGAGATGTTCTGG-3′ primers, producing a 170-bp (unspliced) and a 144-bp fragment (spliced) that were separated on a 2% of agarose gel.

Microarray data

The present expression profile data are available at GEO as GSE16649.

Results

Search for genes associated with metastatic potential in human lung cancer cells

In the present study, we first compared the gene expression profile of a highly metastatic LNM35 clone with that of a low metastatic parental clone, N15, which was also derived from NCI-H460 (13). Consequently, 6 genes, including 2 previously uncharacterized transcripts corresponding to an EST clone (T70922) and LOC441052, determined on the basis of a membrane microarray annotation, were found to be differentially expressed (Supplementary Table S1). Those 2 uncharacterized transcripts were selected for further analysis by quantitative PCR analysis using L2D2, a revertant clone of LNM35 with low metastatic characteristics (12). We found that a transcript corresponding to T70922 was downregulated in L2D2 in association with the loss of metastatic ability. A subsequent *in silico* search using the EST clone revealed that the putative entire open reading frame covering T70922 was FLJ11051 (Genebank accession# AK001913), based on the corresponding full length cDNA clone.

Inhibition of metastatic phenotype of highly metastatic LNM35 cells *in vivo*

We initially generated knockdown clones of the identified candidate gene with potential activities related to cancer invasion and metastasis (hereafter, referred to as *CIM*, also called *ERLEC1*; ref. 31) using highly metastatic LNM35 cells by stably introducing shRNA (shCIM–LNM35 series), which produced clones with about a 5-fold reduction in CIM expression (Supplementary Fig. S1) when compared with the control clones (VC–LNM35 series). Two control and 3 CIM knockdown clones of LNM35 were then injected into 6-week-old SCID (severe combined immune deficient) mice to investigate their effects on the metastatic capabilities of LNM35. All of the shCIM–LNM35 clones exhibited markedly diminished metastatic capabilities via lymphogenous routes (Fig. 1A, left graph), whereas lung metastatic nodules of shCIM–LNM35 clones were significantly reduced in both number and size (Fig. 1A, middle graph and right photos). There were no distinctions in terms of *in vivo* growth at the primary sites (Fig. 1A, right graph).

Analyses of subcellular localization of CIM

The *CIM* gene encodes a protein consisting of 483 amino acids with a mannose 6-phosphate receptor homology domain and HR to OS-9, which was previously isolated as a gene overexpressed in osteosarcomas (Fig. 1B, left; ref. 32). Although 2.5-kb-sized *CIM* transcripts were abundantly present in adult testis, skeletal muscle, pancreas, and prostate tissues (Supplementary Fig. S2), 9 of 17 (53%) cell lines and 4 of 16 (25%) primary lung tumors obtained from patients exhibited increased *CIM* expression when compared with normal lung tissues (Supplementary Fig. S3A and B). We further examined the expression of *CIM* using our microarray dataset (10) and found that upregulation of *CIM* by more than 2-fold as compared with normal lung tissue was present in 23 of 149 (15.4%) non-small cell lung cancer cases (Supplementary Fig. S3C). The PSORT program (http://psort.ims.u-tokyo.ac.jp/) predicted subcellular localization of CIM to be most likely in the ER. To confirm this prediction, we first constructed a myc-tagged CIM expression vector, as there are no CIM-specific antibodies presently available. As shown in Figure 1C, staining with the anti-myc antibody together with those for ER or Golgi detection clearly demonstrated that CIM localizes mainly in ER. In addition, the use of 2 artificial truncation mutants lacking each of the 2 HRs to OS-9 (Fig. 1B, right) revealed that the

Published OnlineFirst November 30, 2010; DOI:10.1158/0008-5472.CAN-10-1055

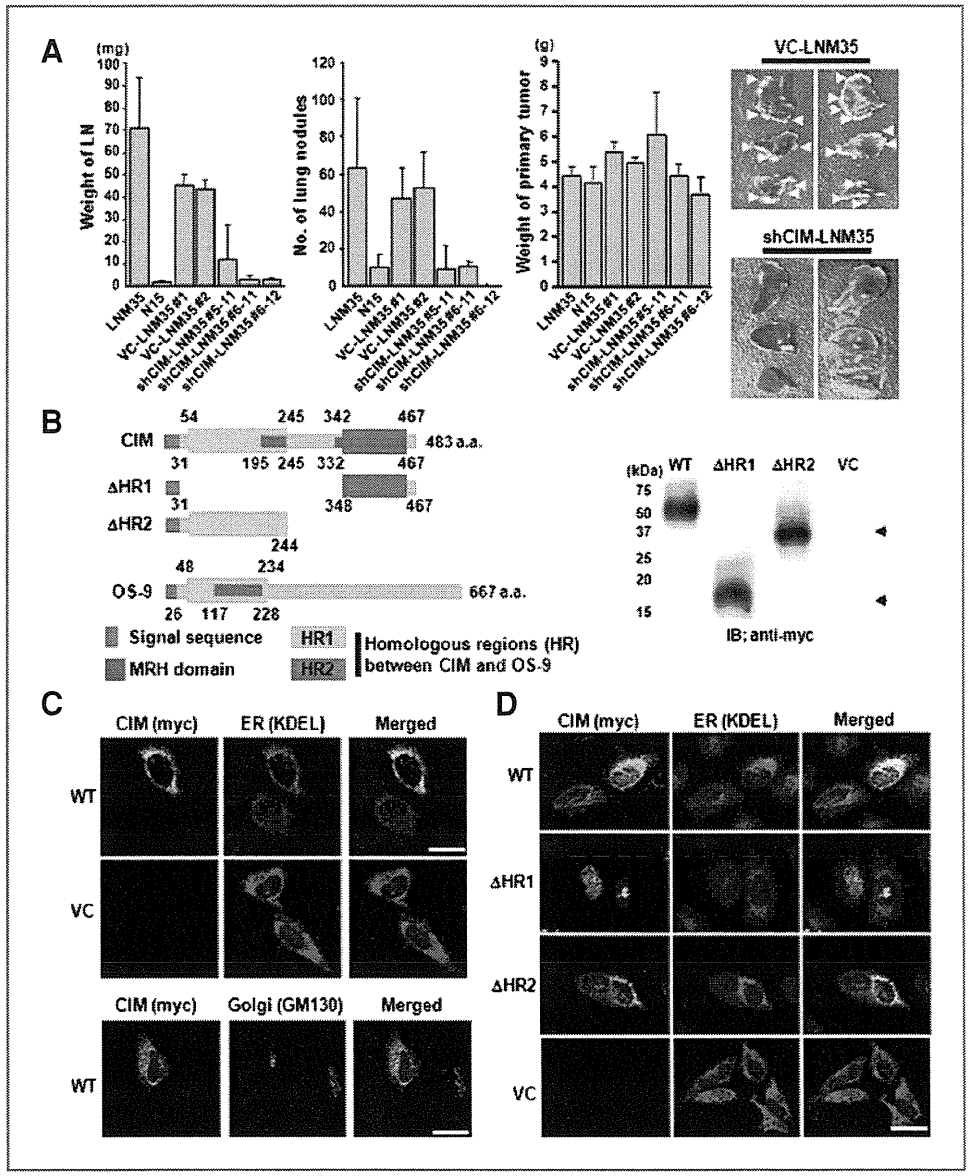

Figure 1. Inhibition of metastatic phenotype of highly metastatic LNM35 cells *in vivo* and *in vitro* by introducing CIM-specific shRNA. A, significant reduction of *in vivo* metastasis was seen via both lymphogenous and hematogenous routes in all 3 LNM35 clones stably transfected with CIM-specific shRNA expression vectors (shCIM-LNM35 #5–11, #6–11, and -12), in comparison with control clones (VC #1 and #2). Values represent lymph node weight (left graph), number of lung metastasis nodules (middle graph), and primary tumor weight (right graph). Error bars denote SD. Representative lung tissues resected from mice inoculated with VC–LNM35 (top photos) and shCIM–LNM35 (bottom photos) cells. Multiple white nodules indicating metastasis were observed in the lungs of VC–LNM35-innoculated mice. B, schematic diagram of the functional domains of CIM in relation to truncation mutants and OS-9. The mannose 6-phosphate receptor homology (MRH) domain and homologous regions (HR) between CIM and OS-9 are indicated. Expression of wild-type and artificial-truncated mutants CIM protein were confirmed. C, CIM was detected in ER, but not in the Golgi apparatus in BEAS-2B normal lung epithelial cells transiently transfected with myc-tagged CIM. D, immunofluorescence staining of wt- and mutant-CIM-transfected BEAS-2B cells, showing requirement of HR1 for subcellular localization of CIM in ER. Scale bars, 10 μm.

N-terminal HR was necessary for its subcellular localization in ER (Fig. 1D).

Identification of a role of CIM in regulation of HIF-1α expression through modulation of OS-9 function.

ER is a key site of protein synthesis and serves a variety of general functions in protein modification. We therefore compared the protein expression profiles between shCIM–LNM35 and VC–LNM35 cells through a proteomic approach by mass spectrometric analysis to gain insight into the molecular function of CIM (Fig. 2A). Among 1,103 unique proteins identified, 27 proteins were upregulated (more than 2-fold) in shCIM–LNM35 cells, whereas 47 proteins were downregulated (less than 2-fold, Supplementary Table S2). We employed KeyMolnet software to explore possible networks affected by CIM and found 39 interrelations involving 42 proteins (Supplementary Fig. S4). We consequently noted that HIF-1 and HIF-1α were centered with several molecules downregulated

Published OnlineFirst November 30, 2010; DOI:10.1158/0008-5472.CAN-10-1055

in shCIM–LNM35 cells (Fig. 2B). On the basis of these results, we speculated that changes in HIF-1α expression in shCIM–LNM35 cells might have been overlooked in our proteomic analysis, even though it is affected by CIM knockdown, possibly because the digested peptides of HIF-1α were coeluted together with those from other highly abundant proteins during liquid chromatography separation. In line with our expectation, comparison of HIF-1α expression between shCIM and VC–LNM35 cells clearly showed downregulation of HIF-1α specifically in shCIM–LNM35 cells under normoxic as well as prolonged hypoxic conditions (Fig. 2C). We further investigated whether treatment with the MG132 proteasome inhibitor affected HIF-1α expression in shCIM–LNM35 cells, and found that acceleration of proteasome-mediated degradation might be involved in the downregulation of HIF-1α in cells knocked down for CIM (Fig. 2D).

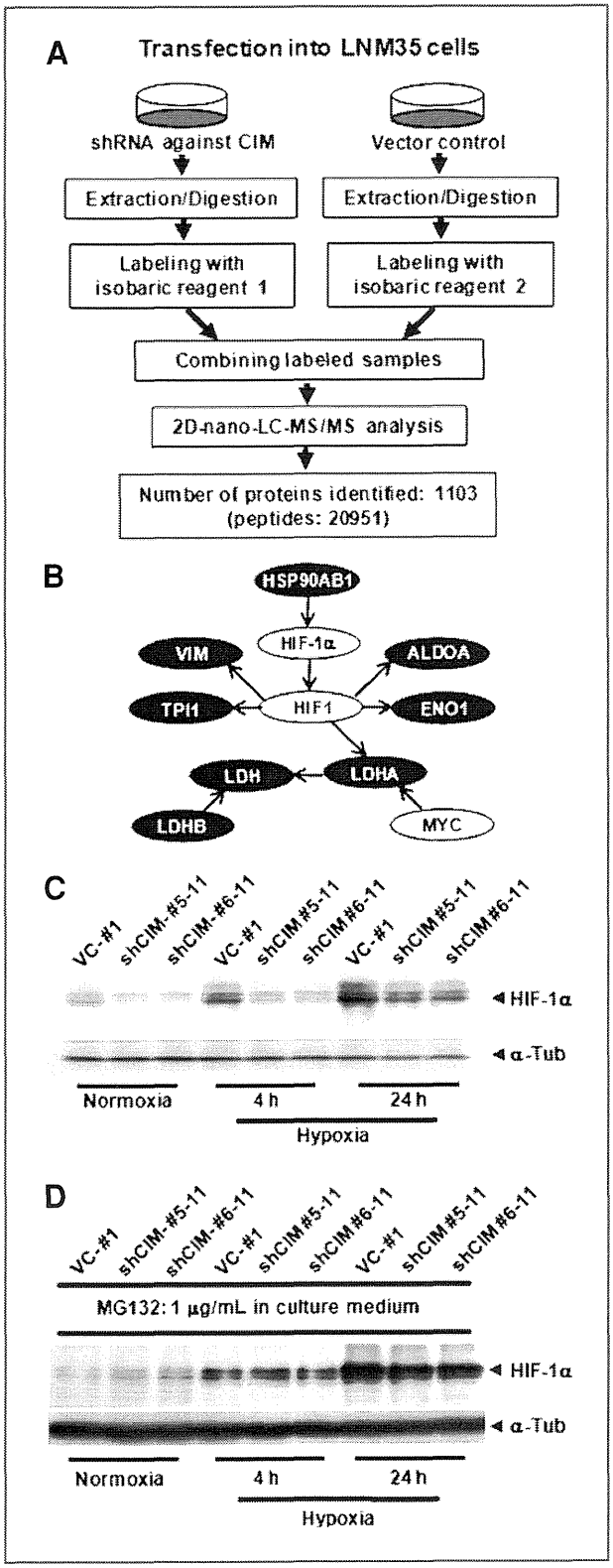

We next sought to verify the influence of CIM on HIF-1α regulation by transfecting CIM-specific siRNA molecules into LNM35 cells, which resulted in a less than 5-fold reduction in CIM expression (supplementary Fig. S5), and found that downregulation of HIF-1α expression was observed in CIM-knockdown cells, while expression of HIF-1ß was not affected (Fig. 3A). Further verification by transiently transfecting CIM into N15 cells, which showed reduced expression of endogenous CIM (Supplementary Fig. S3A), was conducted and the results obtained revealed a positive effect of CIM on HIF-1α expression (Fig. 3B). Next, we investigated the effects of CIM on proliferation under hypoxic condition. N15 cells were transiently transfected with either control or CIM-expression vectors, then cultured under normoxic or hypoxic conditions for the indicated time periods. Cell viability was analyzed by MTT analysis and we found that exogenous expression of CIM resulted in acquisition of tolerance-to-hypoxia (Fig. 3C). To investigate whether tolerance-to-hypoxia in CIM-transfected N15 cells is due to upregulation of HIF-1α, we transfected HIF-1α–specific siRNA into N15 cells expressing exogenous CIM. Knockdown of HIF-1α eliminated the acquisition of tolerance-to-hypoxia in N15 cells induced by CIM (Fig. 3D). To investigate the relationship between CIM and HIF-1α *in vivo*, Western blot analysis of HIF-1α expression was performed using both primary and metastatic tumors in the lungs of mouse xenografts of VC- and shCIM–LNM35 clones. We clearly detected reduced HIF-1α expression at the primary tumor sites of the xenografts of the shCIM–LNM35 clones, as compared with the VC–LNM35 clones (Supplementary Fig. S6A). In contrast, HIF-1α was shown to be expressed in metastatic nodules in the lungs of the shCIM–LNM35 clones at a level noticeably closer to that observed in the

Figure 2. Identification of positive regulation of HIF-1α expression by CIM. A, schematic diagram of strategy used for proteomic identification of CIM-regulated proteins. B, network analysis of proteins differentially expressed between LNM35 cells stably knocked down for CIM (shCIM) and corresponding empty vector control (VC) cells using KeyMolnet software based upon proteomic profiling. A selected portion surrounding HIF-1α is shown (see also Supplementary Fig. S4). Closed circles are proteins whose differential expression were observed through proteomic analyses. Open circles, selected by pathway analysis with KeyMolnet. C, Western blot analysis of HIF-1α expression, showing its reduction in shCIM under both normoxic and hypoxic conditions (O_2 concentration; 0.5%). D, Western blot analysis of HIF-1α in the presence of a proteasome inhibitor, MG132, in shCIM and VC cells. Note that the CIM knockdown-mediated reduction of HIF-1α expression was abrogated in the presence of MG132. α-tubulin, loading control.

Published OnlineFirst November 30, 2010; DOI:10.1158/0008-5472.CAN-10-1055

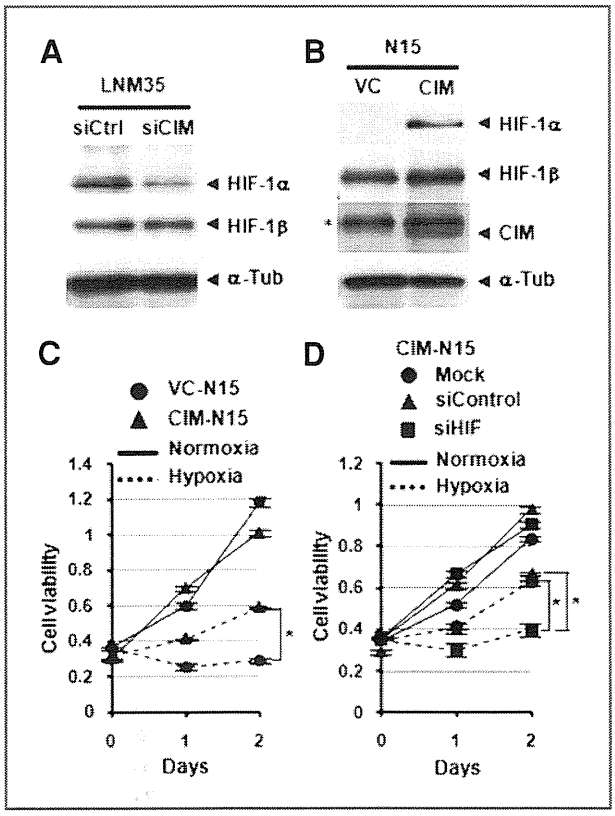

Figure 3. Positive regulation of HIF-1α expression by CIM leads cancer cells to the tolerance-to-hypoxia. A, the influence of CIM on HIF-1α regulation was verified by transfecting CIM-specific siRNA molecules into LNM35 cells. B, Western blot analysis of HIF-1α in N15 cells transiently transfected with myc-tagged CIM. CIM expression was analyzed using the anti-c-myc antibody. α-tubulin, loading control. *, nonspecific cross-reaction. C, results of MTT assay of N15 cells exogenously expressing CIM (CIM-N15) and control cells (VC-N15), showing acquisition of tolerance-to-hypoxia by CIM. D, results of MTT assay of N15 cells exogenously expressing CIM (CIM-N15), which were further transfected with either HIF-1α-specific or control siRNA, showing that tolerance-to-hypoxia is diminished by knockdown of HIF-1α in CIM-N15 cells.

metastatic nodules of the VC–LNM35 clones (Supplementary Fig. S6B).

Our findings revealed that CIM played a role in positive regulation of HIF-1α expression. CIM is known to have homology with OS-9, which play a role in regulation of HIF-1α (27), accordingly we examined whether CIM functioned with OS-9. 293T cells were transiently transfected with wild-type or HR-truncated myc-tagged expression vectors of CIM, and subjected to immunoprecipitation followed by Western blot analysis with anti-myc and anti-OS-9 antibodies. It was clearly shown that wild-type CIM interacted with OS-9 and that both HRs were necessary for the interaction (Fig. 4A, top and bottom left). Since HR1 also appears to play a role in regulation of the subcellular localization of CIM (Fig. 1D), it is possible that there are multiple functional domains within the HR1 region, including those for interactions with ER and OS-9. Accordingly, a future study delineating domains responsible for each interaction to clarify how CIM sequesters OS-9 in the ER would be interesting. We did not detect any interactions of CIM with either HIF-1α or PHD2 (Fig. 4A, top right, and bottom middle, and right), indicating that CIM binds only to OS-9 in the complex implicated in the degradation of HIF-1α protein. We further analyzed whether the interaction between OS-9 and CIM modifies the complex formation and found that the exogenous expression of CIM noticeably reduced the interaction between HIF-1α and OS-9, leading to upregulation of HIF-1α expression detected in whole cell lysates (Fig. 4B). We also observed that transfection of OS-9–specific siRNA molecules into N15 cells, which showed reduced expression of endogenous CIM (Supplementary Fig. S3A), resulted in upregulation of HIF-1α expression (Fig. 4C). Furthermore, transfection of CIM-specific siRNA into LNM35 cells followed by transfection of either OS-9-specific or control siRNA revealed that downregulation of HIF-1α by siCIM is diminished by knockdown of OS-9 (Fig. 4D, left).

Next, we analyzed the effects of CIM together with OS-9 on proliferation under hypoxic condition using LNM35 cells. shCIM–LNM35 cells were transiently transfected with either OS-9-specific or control siRNA, then cultured under normoxic or hypoxic conditions for the indicated time periods, and cell viability was analyzed by MTT analysis. We observed that knockdown of OS-9 partially alleviated hypoxia-induced growth retardation in LNM35 cells knocked down for CIM (Fig. 4D, right). Accordingly, our observations suggested that CIM has an ability to regulate HIF-1α through sequestration of OS-9 from a complex with HIF-1α and PHD2, leading to inhibition of HIF-1α degradation and its consequential upregulation, and affect the tolerance-to-hypoxia, which may suppress tumor cells to proliferate in metastatic site.

Identification of another role of CIM for UPR

Proteomic analyses also revealed that elevated expressions of proteins implicated in protein folding, maturation, and transport, such as HSPB1, GRP75, and LGALS3 (33–35), in shCIM–LNM35 cells, which we verified by Western blot analysis (Fig. 5A). Furthermore, bioinformatic analysis revealed that GO term identifiers for the biological processes related to UPR (cellular response to ER stresses, $P = 0.0122$), glycolysis ($P = 0.0129$), and the protein metabolic process ($P = 0.0228$) were observed more frequently than expected ($P < 0.05$) in the 74 proteins affected by CIM (Supplementary Table S3). Since some ER resident proteins are suggested to play roles in acquisition of aggressive phenotypes of human cancers by conferring adaptation of tumors to the microenvironment (21, 23, 36), we speculated that CIM may also have an effect on the regulation of homeostasis of ER functions, modulating metastatic capability.

First, we analyzed the effects of CIM on proliferation under an ER-stressed condition induced by tunicamycin treatment and found a significant reduction in the growth of shCIM–LMN35 cells (Fig. 5B), which was accompanied with increased levels of cleaved caspases-3 and -8, and PARP (Fig. 5C), indicating that knockdown for CIM sensitized the LNM35 cells to the ER stress. Interestingly, we also observed an apparently impaired induction of BiP (Fig. 5D upper panel), which is normally induced as a part of the manifestation of

Published OnlineFirst November 30, 2010; DOI:10.1158/0008-5472.CAN-10-1055

cytoprotective UPR signaling mediated by IRE1α (21), in tunicamycin-treated shCIM–LNM35 cells. Furthermore, activation of phosphorylation of IRE1α and ERK was also repressed, indicating that CIM is required for transduction of the adaptive signals in UPR (Fig. 5D upper panel). We observed that IRE1α-mediated splicing of XBP-1 was clearly repressed in shCIM–LNM35 cells exposed to tunicamycin, reflecting impaired ER stress signaling through IRE1α (Fig. 5D lower panel), whereas phosphorylation of p38, which occurs in response to ER stress, was found to be modestly affected (Supplementary Fig. S7).

BiP is a key molecule in ER, which binds to IRE1α in nonstressed cells and maintains them in an inactive form, whereas accumulated unfolded proteins pull BiP away from IRE1α and triggers the downstream pathway of the UPR (37). Immunoprecipitation–Western blot analysis clearly demonstrated coimmunoprecipitation of BiP with myc-tagged CIM regardless of the presence of tunicamycin, whereas IRE1α was not present in the anti-myc immunoprecipitates (Fig. 6A). Further investigation using immunoprecipitation with the anti-BiP antibody and subsequent Western blot analysis with the anti-IRE1α antibody revealed that dissociation of BiP from IRE1α in response to ER stress was markedly inhibited in LNM35 cells knocked down for CIM (Fig. 6B). Although ER stresses imposed by an insufficient microenvironment have been suggested to play a suppressive role in the proliferation of cancer cells at metastatic sites (22, 23), the present observations suggest that CIM confers tolerance to such ER stresses in cancer cells at metastatic sites and play a role in formation of metastasis, by allowing them to survive at metastatic sites.

Discussion

Cancer cells acquire abilities to cope with cellular stresses caused by an insufficient microenvironment in terms of nutrient supply, pH, and oxygenation, which eventually lead to their aggressive growth, metastasis, and poor response to therapy, and a number of cellular responses that have vital roles in survival under such stress conditions are thought to be crucially involved in this process. Among such stress responses the best understood is the one mediated by the hypoxia inducible transcription factor, HIF-1α, which activates the transcription of various target genes involved in angiogenesis, cell proliferation, invasion, and metastasis (25, 38). In addition, the complex and multifaceted signal-transduction cascade of UPR, which serves to limit the accumula-

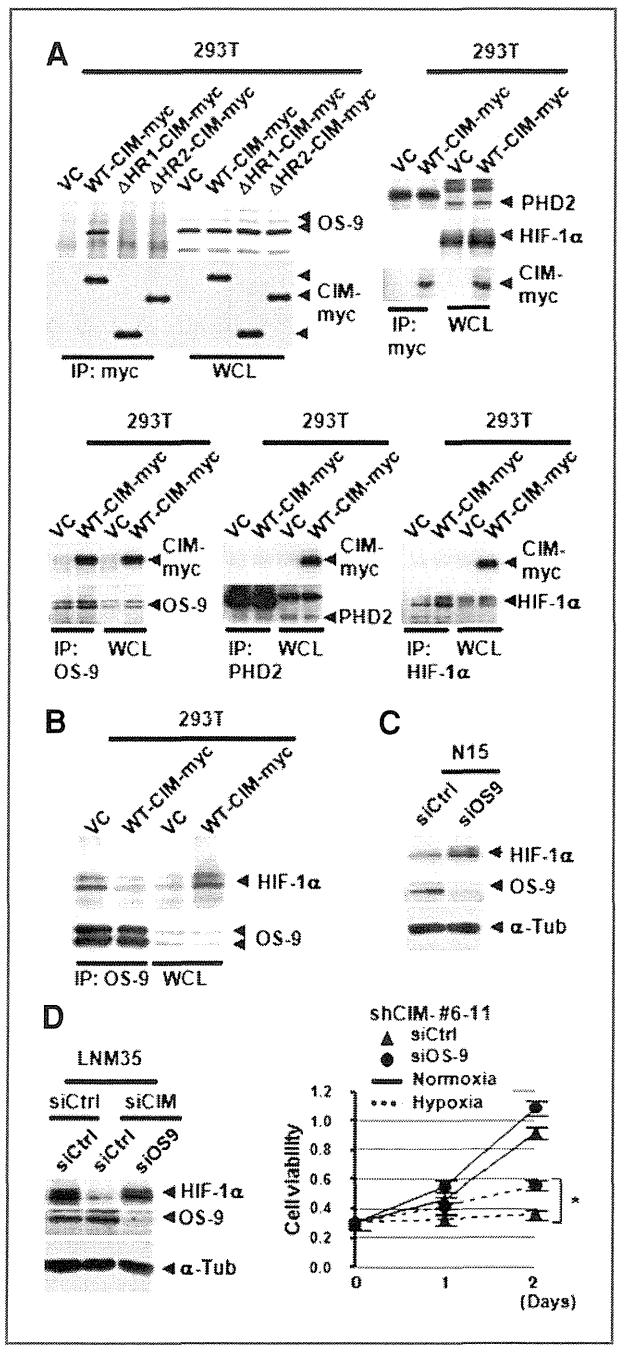

Figure 4. Interaction of CIM with a negative regulator of HIF-1α, OS-9, and CIM-mediated inhibition of the interactions between OS-9 and HIF-1α. A, IP-Western blot analysis of the interactions between CIM and OS-9, showing the necessity of both OS-9 homologous regions in 293T cells transiently transfected with CIM (upper and lower left panels). For structural configurations of wild-type (WT) and mutant CIM (ΔHR1-CIM and ΔHR2-CIM), see Figure 1B. Immunoprecipitates (IP)–Western blot analysis of the interactions of CIM with PHD2 and HIF-1α in CIM-transfected 293T cells, showing lack of interactions (upper right, and lower middle and right panels). B, IP-Western blot analysis of the interactions between OS-9 and HIF-1α in 293T cells transfected with CIM, showing a noticeable decrease in the interactions between OS-9 and HIF-1α. Note that HIF-1α expression was increased in CIM-transfected cells in whole cell lysates. WCL, whole cell lysate. C, influence of CIM and OS-9 expression on HIF-1α regulation. Western blot analysis of N15 cells transfected with OS-9–specific siRNA showed increased HIF-1α expression. D, Western blot analysis of HIF-1α in LNM35 cells transiently transfected with CIM-specific siRNA (siCIM) followed by OS-9–specific siRNA (siOS9) or control siRNA (siCtrl) showed diminished effects of siCIM on HIF-1α expression in LNM35 cells followed by OS-9 knockdown (left panel). Results of MTT assay of LNM35 cells transfected with CIM-specific shRNA (shCIM #6–11) followed by either siOS9 or control siCtrl showed that knockdown of OS-9, known to be involved in HIF-1α degradation, partially alleviated hypoxia-induced growth retardation in LNM35 cells knocked down for CIM (right graph).

Published OnlineFirst November 30, 2010; DOI:10.1158/0008-5472.CAN-10-1055

tion of misfolded proteins and also regulate programmed cell death, is another important mechanism to relieve stress imposed by the surrounding insufficient microenvironment (21, 22, 24). The notion that hypoxia-induced HIF-1α-mediated response and UPR may have a functional link has recently attracted much attention (39, 40), raising it as a key issue to further elucidate which pathway(s) and molecule(s) are involved in this new aspect of connection to stress responses. Our present findings demonstrate that CIM has multifaceted roles in 2 distinct stress responses, that is, regulation of HIF-1α expression and modulation of UPR, thus providing another layer to the link between the 2 stress responses (Supplementary Fig. S8).

HIF-1α is an oxygen-dependent transcriptional factor that plays important roles in enabling cells to survive in hypoxic conditions, as it activates the transcription of various target genes involved in angiogenesis, cell proliferation, invasion, and metastasis (25, 38). A previous study showed that proteasome-mediated degradation of HIF-1α is negatively regulated by OS-9, which carries regions homologous with CIM, through modulation of the formation of a complex between HIF-1α and PHDs leading to recruitment of VHL and eventual proteasomal degradation of HIF-1α (27). The present study clearly demonstrated that CIM positively regulates HIF-1α expression by inhibiting its degradation through interaction with the negative regulator OS-9 and confers lung cancer cells tolerance-to-hypoxia allowing proliferation in a hypoxic condition. Given that HIF-1α is thought to play critical roles in tumor progression (25, 38), it is conceivable that CIM contributes to promotion of aggressive growth of tumor cells in metastatic sites, in which cells must survive with a low supply of oxygen provided from the surrounding microenvironment, by positively regulating HIF-1α.

The UPR process has been suggested to poise cancer cells between apoptotic responses, dormancy, and aggressive growth, however, it remains to be clarified how it is controlled and which molecules are involved (21, 22, 24). Results of our proteomic GO term analysis suggest a possible link between CIM and another important cellular stress response, UPR. We further demonstrated that CIM is involved in ER stress-induced dissociation of BiP, a major ER chaperon with a key role in UPR, from IRE1α and consequential activation BiP and ERK, which protects cells from apoptotic cell death under ER-stressed conditions (36, 41). These findings suggest that CIM may contribute to tumor progression by protecting lung cancer cells from apoptosis under ER-stressed conditions, which are

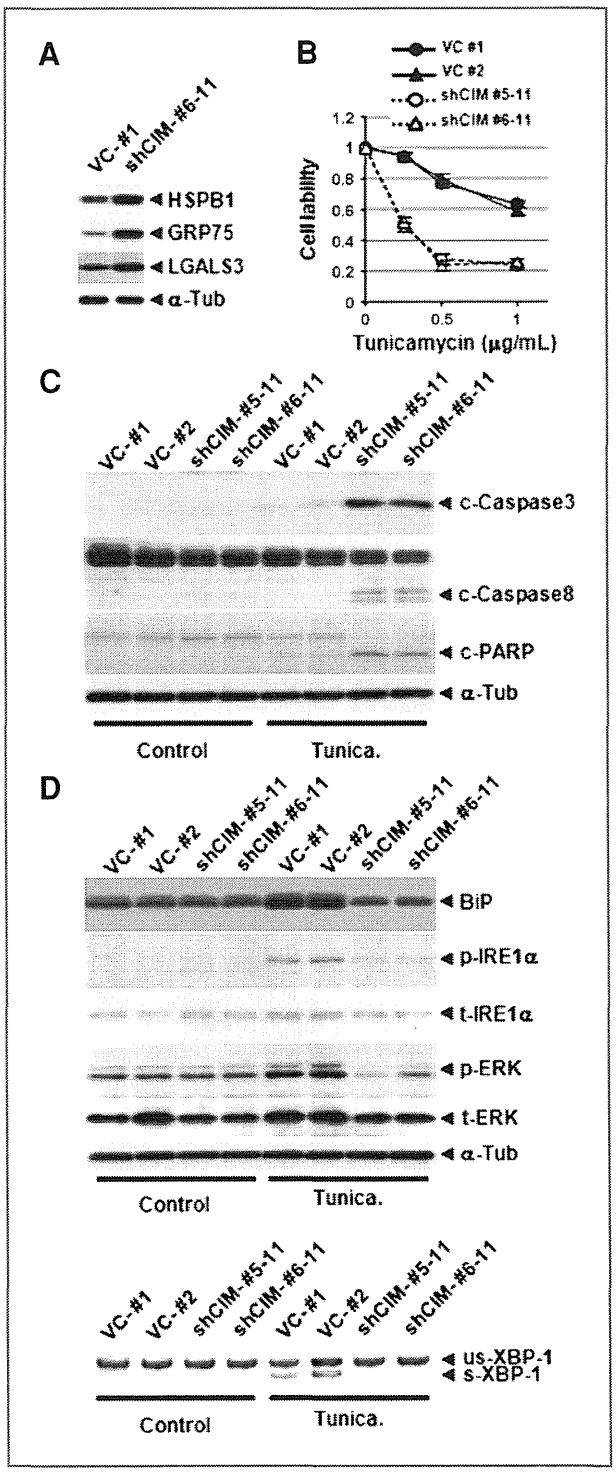

Figure 5. Cytoprotective role of CIM in cancer cells under ER stress condition. A, Western blot verification of differential expression of proteins, which were identified as upregulated in LNM35 knocked down for CIM (shCIM–LNM35) cells by proteomic analysis. B, results of MTT assay of LNM35 knocked down for CIM (shCIM #5–11 and #6–11) and control clones (VC #1 and #2), showing sensitization to tunicamycin by shCIM clones. C, Western blot analysis of cleaved-caspase-3 (c-Caspase3), -caspase-8 (c-Caspase8), and -PARP (c-PARP) expressions in shCIM and VC clones cultured in the presence or absence of tunicamycin. Arrowheads indicate cleaved forms. D, Western blot analysis of BiP, total and phosphorylated-IRE1α (t- and p-IRE1α, respectively), and total and phosphorylated-ERK (t- and p-ERK, respectively) expressions in shCIM and VC clones cultured in the presence or absence of tunicamycin (upper panel). XBP-1 splicing analysis was performed with RT-PCR using primers, which were used to amplify a fragment of XBP-1 harboring the region of IRE1α-mediated splicing. XBP-1 splicing in cells exposed to tunicamycin was clearly repressed in shCIM–LNM35 cells, which indicated impaired ER stress signaling through IRE1α (bottom).

Published OnlineFirst November 30, 2010; DOI:10.1158/0008-5472.CAN-10-1055

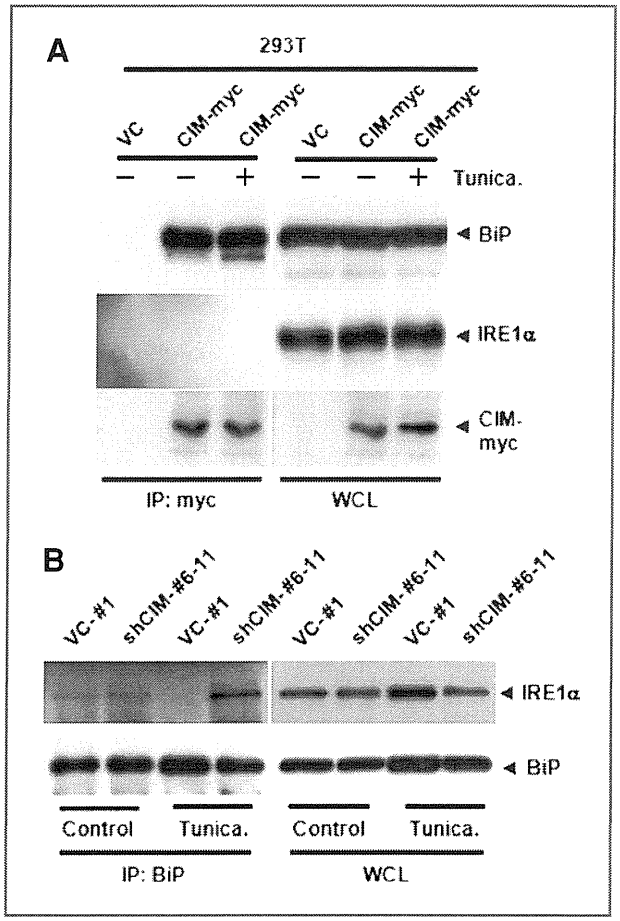

Figure 6. Molecular mechanism of CIM in regulation of unfolded protein response. A, Immunoprecipitation (IP)–Western blot analysis for the detection of BiP and IRE1α proteins in anti-myc antibody immunoprecipitates (IP: myc) from whole cell lysates of myc-tagged CIM transfected 293T cells. Note the specific interaction of myc-tagged CIM with BiP, but not with IRE1α. B, IP–Western blot analysis for the detection of interactions between BiP and IRE1α protein in WCL prepared from shCIM and VC clones of LNM35 cultured in the presence or absence of tunicamycin. Note the persistent binding of BiP with IRE1α in the presence of tunicamycin in shCIM #6–11 clone, in contrast to their dissociation in the VC #1 clone.

conceivably encountered by cancer cells in the process of metastasis (36). It is also important to note that while *ERLEC1*, synonymous with *CIM* and originally identified as a Krm2-binding protein, has been shown to function in N-glycan recognition in ER with a possible role in glycoprotein traffic and organogenesis in Xenopus (31), *XTP3B/c2orf30* (also synonymous with *CIM*) was later reported to form a quality control complex in ER, thus eliminating misfolded proteins through ubiquitination in the ER (42, 43). Our findings indicate that CIM/ERLEC1/XTP3-B plays another distinct function at ER by sequestering BiP and consequentially modulating IRE1α-mediated ER stress signals, suggesting a buffering role of CIM in the regulation of UPR initiated by ER luminal stress, after which it is transmitted to the cytosol and nucleus.

The present results provide evidence of another layer to the link between hypoxia-induced HIF-1α-mediated response and UPR via the multifaceted roles of CIM, which were identified in our search for a gene involved in metastatic processes of lung cancer. Emerging evidence indicates that agents that inhibit HIF-1α and/or key UPR signaling molecules could define a new type of cancer therapy that prevents adaptation of tumors to a hostile environment (25, 44). Given that it has multifaceted roles in these signaling pathways, further clarification of the functional roles of CIM including that in normal cells under physiological conditions is apparently warranted. Those results should provide insight into how cancer cells acquire metastatic capabilities for survival and colonization at metastatic sites under stressful conditions, which may ultimately aid in development of a novel therapeutic strategy aimed at reducing the large number of deaths caused by this devastating disease.

Disclosure of Potential Conflicts of Interest

No potential conflicts of interests were disclosed.

Acknowledgments

We thank Yoshio Tatematsu and Tomoko Harano for their excellent technical help.

Grant Support

This work was supported in part by a Grant-in-Aid for Scientific Research on Priority Areas from the Ministry of Education, Culture, Sports, Science and Technology of Japan, and a Grant-in-Aid for Exploratory Research and Program for Improvement of Research Environment for Young Researchers from Special Coordination Funds for Promoting Science and Technology commissioned by the Ministry of Education, Culture, Sports, Science and Technology of Japan.

Received 03/26/2010; revised 09/12/2010; accepted 10/04/2010; published OnlineFirst 11/30/2010.

References

1. Takahashi T, Sidransky D. Biology of lung cancer. In: Mason R, Broaddus V, Murray J, Nadel J, editors. Textbook of Respiratory Medicine 4th edition. 15th ed. Philadelphia: Elsevier Science; 2005. p. 1311–27.
2. Giaccone G. Clinical impact of novel treatment strategies. Oncogene 2002;21:6970–81.
3. Ramaswamy S, Ross KN, Lander ES, Golub TR. A molecular signature of metastasis in primary solid tumors. Nat Genet 2003;33:49–54.
4. Pantel K, Brakenhoff RH. Dissecting the metastatic cascade. Nat Rev Cancer 2004;4:448–56.
5. Clark EA, Golub TR, Lander ES, Hynes RO. Genomic analysis of metastasis reveals an essential role for RhoC. Nature 2000;406:532–5.
6. Minn AJ, Gupta GP, Siegel PM, Bos PD, Shu W, Giri DD, et al. Genes that mediate breast cancer metastasis to lung. Nature 2005;436:518–24.
7. Glinsky GV, Berezovska O, Glinskii AB. Microarray analysis identifies a death-from-cancer signature predicting therapy failure in patients with multiple types of cancer. J Clin Invest 2005;115:1503–21.
8. Tomida S, Yanagisawa K, Koshikawa K, Yatabe Y, Mitsudomi T, Osada H, et al. Identification of a metastasis signature and the DLX4 homeobox protein as a regulator of metastasis by combined transcriptome approach. Oncogene 2007;26:4600–8.
9. Tomida S, Takeuchi T, Shimada Y, Arima C, Matsuo K, Mitsudomi T, et al. Relapse-related molecular signature in lung adenocarcinomas identifies patients with dismal prognosis. J Clin Oncol 2009;27:2793–9.

Published OnlineFirst November 30, 2010; DOI:10.1158/0008-5472.CAN-10-1055

10. Takeuchi T, Tomida S, Yatabe Y, Kosaka T, Osada H, Yanagisawa K, et al. Expression profile-defined classification of lung adenocarcinoma shows close relationship with underlying major genetic changes and clinicopathologic behaviors. J Clin Oncol 2006;24:1679–88.
11. Koshikawa K, Osada H, Kozaki K, Konishi H, Masuda A, Tatematsu Y, *et al. Significant up-regulation of a novel gene, CLCP1, in a highly* metastatic lung cancer subline as well as in lung cancers *in vivo*. Oncogene 2002;21:2822–8.
12. Kozaki K, Koshikawa K, Tatematsu Y, Miyaishi O, Saito H, Hida T, et al. Multi-faceted analyses of a highly metastatic human lung cancer cell line NCI-H460-LNM35 suggest mimicry of inflammatory cells in metastasis. Oncogene 2001;20:4228–34.
13. Kozaki K, Miyaishi O, Tsukamoto T, Tatematsu Y, Hida T, Takahashi T, et al. Establishment and characterization of a human lung cancer cell line NCI-H460-LNM35 with consistent lymphogenous metastasis via both subcutaneous and orthotopic propagation. Cancer Res 2000;60:2535–40.
14. Hanash S. Disease proteomics. Nature 2003;422:226–32.
15. Aebersold R, Mann M. Mass spectrometry-based proteomics. Nature 2003;422:198–207.
16. Yanagisawa K, Shyr Y, Xu BJ, Massion PP, Larsen PH, White BC, et al. Proteomic patterns of tumour subsets in non-small-cell lung cancer. Lancet 2003;362:433–9.
17. Yanagisawa K, Tomida S, Shimada Y, Yatabe Y, Mitsudomi T, Takahashi T. A 25-signal proteomic signature and outcome for patients with resected non-small-cell lung cancer. J Natl Cancer Inst 2007;99:858–67.
18. Bantscheff M, Eberhard D, Abraham Y, Bastuck S, Boesche M, Hobson S, *et al. Quantitative chemical proteomics reveals mechan*isms of action of clinical ABL kinase inhibitors. Nat Biotechnol 2007;25:1035–44.
19. Keller M, Ruegg A, Werner S, Beer HD. Active caspase-1 is a regulator of unconventional protein secretion. Cell 2008;132:818–31.
20. Taguchi A, Yanagisawa K, Tanaka M, Cao K, Matsuyama Y, Goto H, et al. Identification of hypoxia-inducible factor-1 alpha as a novel target for miR-17–92 microRNA cluster. Cancer Res 2008;68: 5540–5.
21. Ma Y, Hendershot LM. The role of the unfolded protein response in tumour development: friend or foe? Nat Rev Cancer 2004;4: 966–77.
22. Kim I, Xu W, Reed JC. Cell death and endoplasmic reticulum stress: disease relevance and therapeutic opportunities. Nat Rev Drug Discov 2008;7:1013–30.
23. Wouters BG, Koritzinsky M. Hypoxia signalling through mTOR and the unfolded protein response in cancer. Nat Rev Cancer 2008;8:851–64.
24. Ron D, Walter P. Signal integration in the endoplasmic reticulum unfolded protein response. Nat Rev Mol Cell Biol 2007;8:519–29.
25. Semenza GL. Targeting HIF-1 for cancer therapy. Nat Rev Cancer 2003;3:721–32.
26. Bruick RK, McKnight SL. A conserved family of prolyl-4-hydroxylases that modify HIF. Science 2001;294:1337–40.
27. Baek JH, Mahon PC, Oh J, Kelly B, Krishnamachary B, Pearson M, et al. OS-9 interacts with hypoxia-inducible factor 1alpha and prolyl hydroxylases to promote oxygen-dependent degradation of HIF-1alpha. Mol Cell 2005;17:503–12.
28. Ivan M, Kondo K, Yang H, Kim W, Valiando J, Ohh M, et al. HIFalpha targeted for VHL-mediated destruction by proline hydroxylation: implications for O2 sensing. Science 2001;292:464–8.
29. Jaakkola P, Mole DR, Tian YM, Wilson MI, Gielbert J, Gaskell SJ, et al. Targeting of HIF-alpha to the von Hippel–Lindau ubiquitylation complex by *O2-regulated prolyl hydroxylation. Science 2001;292:468–72.*
30. Ashburner M, Ball CA, Blake JA, Botstein D, Butler H, Cherry JM, et al. Gene ontology: tool for the unification of biology. The gene ontology consortium. Nat Genet 2000;25:25–9.
31. Cruciat CM, Hassler C, Niehrs C. The MRH protein Erlectin is a member of the endoplasmic reticulum synexpression group and functions in N-glycan recognition. J Biol Chem 2006;281: 12986–93.
32. Su YA, Hutter CM, Trent JM, Meltzer PS. Complete sequence analysis of a gene (OS-9) ubiquitously expressed in human tissues and amplified in sarcomas. Mol Carcinog 1996;15:270–5.
33. Guo K, Liu Y, Zhou H, Dai Z, Zhang J, Sun R, et al. Involvement of protein kinase C beta-extracellular signal-regulating kinase 1/2/p38 mitogen-activated protein kinase-heat shock protein 27 activation in hepatocellular carcinoma cell motility and invasion. Cancer Sci 2008;99:486–96.
34. Tsutsumi S, Neckers L. Extracellular heat shock protein 90: a role for a molecular chaperone in cell motility and cancer metastasis. Cancer Sci 2007;98:1536–9.
35. Liu FT, Rabinovich GA. Galectins as modulators of tumour progression. Nat Rev Cancer 2005;5:29–41.
36. Jamora C, Dennert G, Lee AS. Inhibition of tumor progression by suppression of stress protein GRP78/BiP induction in fibrosarcoma B/C10ME. *Proc Natl Acad Sci USA 1996;93:7690–4.*
37. Okamura K, Kimata Y, Higashio H, Tsuru A, Kohno K. Dissociation of Kar2p/BiP from an ER sensory molecule, Ire1p, triggers the unfolded protein response in yeast. Biochem Biophys Res Commun 2000;279:445–50.
38. Zhong H, De Marzo AM, Laughner E, Lim M, Hilton DA, Zagzag D, et al. Overexpression of hypoxia-inducible factor 1alpha in common human cancers and their metastases. Cancer Res 1999;59:5830–5.
39. Zhu K, Chan W, Heymach J, Wilkinson M, McConkey DJ. Control of HIF-1alpha expression by eIF2 alpha phosphorylation-mediated translational repression. Cancer Res 2009;69:1836–43.
40. Bi M, Naczki C, Koritzinsky M, Fels D, Blais J, Hu N, et al. ER stress-regulated translation increases tolerance to extreme hypoxia and promotes tumor growth. EMBO J 2005;24:3470–81.
41. Aguirre-Ghiso JA, Estrada Y, Liu D, Ossowski L. ERK(MAPK) activity as a determinant of tumor growth and dormancy; regulation by p38 (SAPK). Cancer Res 2003;63:1684–95.
42. Christianson JC, Shaler TA, Tyler RE, Kopito RR. OS-9 and GRP94 deliver mutant alpha1-antitrypsin to the Hrd1-SEL1L ubiquitin ligase complex for ERAD. Nat Cell Biol 2008;10:272–82.
43. Hosokawa N, Wada I, Nagasawa K, Moriyama T, Okawa K, Nagata K. Human XTP3-B forms an endoplasmic reticulum quality control scaffold with the HRD1-SEL1L ubiquitin ligase complex and BiP. J Biol Chem 2008;283:20914–24.
44. Kong D, Park EJ, Stephen AG, Calvani M, Cerdellina JH, Monks A, et al. Echinomycin, a small-molecule inhibitor of hypoxia-inducible factor-1 DNA-binding activity. Cancer Res 2005;65:9047–55.

Published OnlineFirst September 22, 2010; DOI:10.1158/0008-5472.CAN-10-0784

AACR

Cancer Research

Regulation of DNA Polymerase POLD4 Influences Genomic Instability in Lung Cancer

Qin Miao Huang, Shuta Tomida, Yuji Masuda, et al.

Cancer Res 2010;70:8407-8416. Published OnlineFirst September 22, 2010.

Published OnlineFirst September 22, 2010; DOI:10.1158/0008-5472.CAN-10-0784

Cancer Research

Regulation of DNA Polymerase POLD4 Influences Genomic Instability in Lung Cancer

Qin Miao Huang[1], Shuta Tomida[1], Yuji Masuda[5], Chinatsu Arima[1], Ke Cao[1], Taka-aki Kasahara[1], Hirotaka Osada[3], Yasushi Yatabe[4], Tomohiro Akashi[2], Kenji Kamiya[5], Takashi Takahashi[1], and Motoshi Suzuki[1]

Abstract

Genomic instability is an important factor in cancer susceptibility, but a mechanistic understanding of how it arises remains unclear. We examined hypothesized contributions of the replicative DNA polymerase δ (pol δ) subunit *POLD4* to the generation of genomic instability in lung cancer. In examinations of 158 lung cancers and 5 mixtures of 10 normal lungs, cell cycle- and checkpoint-related genes generally showed mRNA expression increases in cancer, whereas *POLD4* showed reduced mRNA in small cell lung cancer (SCLC). A fraction of non–small cell lung cancer patients also showed low expression comparable with that in SCLC, which was associated with poor prognosis. The lung cancer cell line ACC-LC-48 was found to have low *POLD4* expression, with higher histone H3K9 methylation and lower acetylation in the *POLD4* promoter, as compared with the A549 cell line with high *POLD4* expression. In the absence of POLD4, pol δ exhibited impaired *in vitro* DNA synthesis activity. Augmenting POLD4 expression in cells where it was attenuated altered the sensitivity to the chemical carcinogen 4-nitroquinoline-1-oxide. Conversely, siRNA-mediated reduction of POLD4 in cells with abundant expression resulted in a cell cycle delay, checkpoint activation, and an elevated frequency of chromosomal gap/break formation. Overexpression of an engineered *POLD4* carrying silent mutations at the siRNA target site rescued these phenotypes, firmly establishing the role of POLD4 in these effects. Furthermore, POLD4 overexpression reduced intrinsically high induction of γ-H2AX, a well-accepted marker of double-stranded DNA breaks. Together, our findings suggest that reduced expression of POLD4 plays a role in genomic instability in lung cancer. *Cancer Res; 70(21); 8407–16. ©2010 AACR.*

Introduction

Lung cancer has become the leading cause of cancer death in many industrialized countries, with small cell lung cancer (SCLC), a very aggressive subset formed by small cells with scarce cytoplasm, molded nuclei, and neuroendocrine differentiation, accounting for about 15% to 20% of all lung cancer cases (1). Due to its highly proliferative and metastatic potential, as well as nearly certain recurrence after chemotherapy, the 5-year survival rate for SCLC is around 5% (2).

It was recently reported that highly conserved DNA damage response pathways are frequently altered at various phases in human cancers (3–8). Activation of DNA damage checkpoints, even in preneoplastic lesions, leads to cell cycle blockade or apoptosis (3, 6), and abrogation of that activation is thought to be critical during multistep transformation processes, whereas fully malignant cells of overt cancers frequently carry various defects in checkpoint mechanisms (4, 5, 7, 8).

In lung cancer, it is conceivable that smoking plays a major role in induction of DNA damage that may be detected by checkpoint responses, although the intrinsic driving force behind this related genomic erosion has yet to be identified (1). For many carcinogens, initiation of carcinogenesis requires DNA replication, suggesting that genetic alterations are fixed in the genome during replication of damaged DNA. For this reason, a long-term hypothesis states that errors in DNA replication and deficits in DNA repair account for multiple mutations in cancer (9, 10). Herein, we report evidence showing that polymerase δ (pol δ), which is a core DNA replication and repair protein, is frequently downregulated in the POLD4 subunit in SCLC and a fraction of non–small cell lung cancer (NSCLC).

Authors' Affiliations: Divisions of [1]Molecular Carcinogenesis and [2]Molecular Mycology and Medicine, Nagoya University Graduate School of Medicine, [3]Division of Molecular Oncology, Aichi Cancer Center Research Institute, and [4]Department of Pathology and Molecular Diagnosis, Aichi Cancer Center Hospital, Nagoya, Japan; and [5]Research Institute for Radiation Biology and Medicine, Hiroshima University, Hiroshima, Japan

Note: Supplementary data for this article are available at Cancer Research Online (http://cancerres.aacrjournals.org/).

Corresponding Author: Motoshi Suzuki, Nagoya University Graduate School of Medicine, Tsuruma-cho 65, Showa-ku, Nagoya 466-8550, Japan. Phone: 81527442455; Fax: 81527442457; E-mail: msuzuki@med.nagoya-u.ac.jp.

doi: 10.1158/0008-5472.CAN-10-0784

Materials and Methods

Cell lines

Cell lines with the prefix ACC-LC- were established in our laboratories. Calu6 and SK-LC-6 cells were generously

Published OnlineFirst September 22, 2010; DOI:10.1158/0008-5472.CAN-10-0784

provided by L.J. Old (Memorial Sloan-Kettering Cancer Center, New York, NY) and PC-10 cells by Y. Hayata (Tokyo Medical University, Tokyo, Japan), whereas the NCI-H460, SK-MES-1, HCT116, and A549 cell lines were purchased from the American Type Culture Collection. Cells were cultured in RPMI 1640 supplemented with 5% fetal bovine serum (Sigma-Aldrich). Plat-E cells were kindly provided by Dr. T. Kitamura (University of Tokyo, Tokyo, Japan). HCT116 and Plat-E cells were cultured in DMEM supplemented with 5% fetal bovine serum.

Antibodies

A polyclonal anti-POLD4 antibody was raised against a purified protein preparation (see Fig. 3B) using a New Zealand White rabbit (Fig. 6A), whereas another polyclonal antibody was raised against a glutathione *S*-transferase (GST)-tagged POLD4 preparation, followed by removal of the anti-GST antibody (CycLex; Fig. 3D). Other antibodies were anti-POLD4 (POLD4/p12 subunit of pol δ) ascites (2B11, Abnova), POLD1 (p125 subunit of pol δ), Chk1 (Santa Cruz Biotechnology), NBS1-pSer343, Chk2-pTyr68, Chk1-pSer317 (Cell Signaling Technology), NBS1 (Oncogene Research/Calbiochem/Merk), ATM-pSer1981 (Rockland Immunochemicals), ATM (2C1, GeneTex, Inc.), H2AX (BL552), SMC1, SMC1-pSer966 (Bethyl laboratories), FLAG (Sigma-Aldrich), Alexa-Fluoro647–conjugated γ-H2AX, p21, p27 (BD), Chk2 (MBL), anti-trimethyl- histone H3 (Lys9), and anti-acetyl-histone H3 (Millipore/Upstate).

Patients

Prior to obtaining patient samples, requisite approval from the review board of Aichi Cancer Center, Nagoya, Japan, and written informed consent from the patients were obtained.

RNA interference

Transfection was carried out using 50 nmol/L of a siRNA (Supplementary Table S1) duplex (Sigma-Aldrich) targeting each mRNA or negative control 1 (Ambion) with Lipofectamine-2000 (Invitrogen).

Quantitative real-time reverse transcriptase-PCR

Total RNA and cDNA were prepared using an RNeasy Mini Kit (QIAGEN) and SuperScript II Reverse Transcriptase (Invitrogen), respectively. Quantitative reverse transcriptase-PCR (RT-PCR) was performed using a 7500 Fast Real-Time PCR System and Power CYBR Green PCR master mix, according to the manufacturer's instructions (Applied Biosystems). The primer sets are described in Supplementary Table S1. Ct values for *POLD4* or *POLD1* were normalized to those of *18S* (ΔCt). The average ΔΔCt values were then calculated by normalization to the ΔCt values of A549 cells.

Chromatin immunoprecipitation

Chromatin immunoprecipitation samples were prepared from A549 or ACC-LC-48 cells logarithmically grown on 10-cm dishes, as previously described (11, 12). The genomic DNA contents were determined by quantitative RT-PCR (Supplementary Table S1). Results were normalized to the input control. SDs are also presented.

Immunoprecipitation of pol δ complexes

Cells were lysed in Nonidet P40 (NP40) lysis buffer [20 mmol/L HEPES (pH 7.8), 300 mmol/L NaCl, 1 mmol/L EDTA, and 1% NP40] supplemented with cOmplete (Roche Diagnostics Gmbh), then centrifuged at 4°C. The anti-POLD1 antibody was added to the supernatant fraction, mixed gently, and incubated overnight at 4°C. After Protein G Sepharose (GE Healthcare) was incubated with the mixture for 1 hour, it was precipitated and washed four times with NP40 lysis buffer. The pol δ complex was recovered from the Sepharose by boiling in SDS sample buffer and was analyzed using Western blotting.

Purification and characterization of pol δ

All proteins used in this study were overproduced in *Escherichia coli* and purified as previously described (13). The purity of the proteins, including 3- and 4-subunit pol δ, was monitored by SDS-PAGE and Coomassie brilliant blue R-250 staining. Protein concentrations were determined using Bio-Rad protein assays with bovine serum albumin (Bio-Rad) as the standard. DNA polymerase activity was measured in a reaction mixture (25 μL) containing 20 mmol/L HEPES-NaOH (pH 7.5), 50 mmol/L NaCl, 0.2 mg/mL bovine serum albumin, 1 mmol/L dithiothreitol, 10 mmol/L $MgCl_2$, 1 mmol/L ATP, 0.1 mmol/L each of dGTP, dATP, dCTP, and [α-^{32}P]dTTP, 33 fmol (240 pmol for nucleotides) of singly primed ss-mp18 DNA (Supplementary Table S1), 1.0 μg (9.1 pmol) of RPA, 86 ng (1.0 pmol as a trimer) of proliferating cell nuclear antigen (PCNA), 75 ng (260 fmol) of RFC, and 11 to 88 ng (46 to 372 fmol) of pol δ. After incubation at 30°C for 10 minutes, the products were electrophoresed on 0.7% alkaline-agarose gels (13).

Plasmid construction and isolation of stable clones

Using an IMAGE clone (ID: 6450262, Invitrogen) and the primer sets (Supplementary Table S1), the *POLD4* open reading frame (ORF) was PCR-cloned, and inserted into the large *Hin*dIII-*Eco*RI fragment of pcDNA3 (FLAGPOLD4pcDNA3). ACC-LC-172 cells were transfected by FLAGPOLD4pcDNA3 and treated with G418 for establishment of stable clones. For construction of an si*D4*-resistant construct, silent mutations were introduced by synthetic oligomers (Supplementary Table S1). The PCR fragments were inserted into a pGFP-MSCV vector (pMSCVpold4). Plat-E cells were transfected using pMSCVpold4 and a VSV-G expression vector, and cultured for two days. The retrovirus was recovered from the culture medium and used for infection. After two days, green fluorescent protein–positive cells were isolated using FACS Vantage or Area2 (BD).

MTT assay

ACC-LC-172 cells and siRNA-treated (48 h) or non-treated cells were separately cultured in 200 μL of culture medium in 96-well plates at a density of 8,000/well. The next day, the medium was replaced with that containing 4-nitroquinoline-1-oxide (4NQO) or vinorelbine, followed by incubation for

Published OnlineFirst September 22, 2010; DOI:10.1158/0008-5472.CAN-10-0784

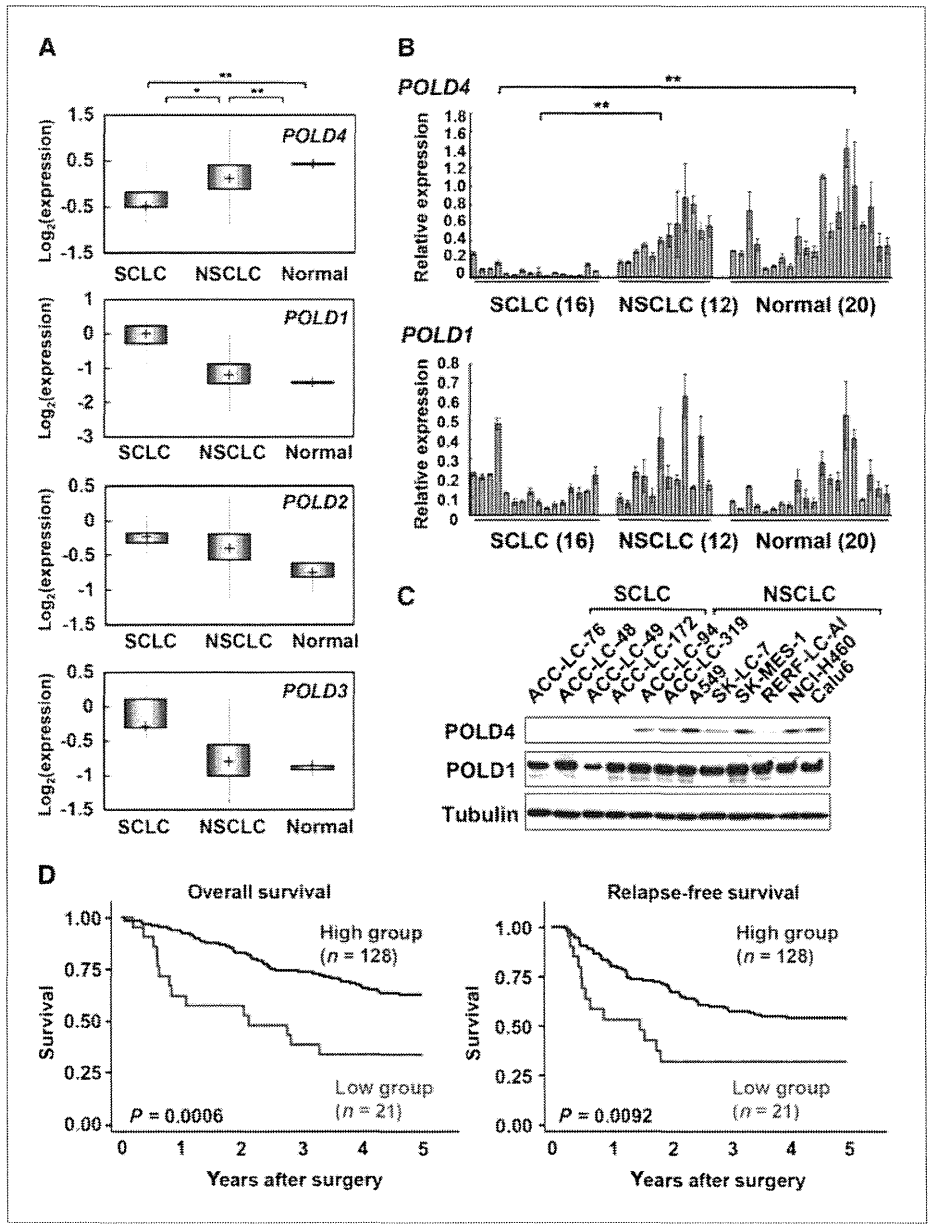

Figure 1. Low expression levels of POLD4 in SCLC. A, microarray analysis of 149 NSCLC, 9 SCLC, and 5 normal lung mixture samples showed that the mRNA expression level of *POLD4*, but not of other pol δ subunits, was low in SCLC. Quartile data are shown in graphs. *, $P < 0.05$; **, $P < 0.01$, *t*-test. B, mRNA expression levels of *POLD4* and *POLD1* in 48 clinical tissue samples, independent of the microarray cohort, were determined by quantitative RT-PCR. The number of each sample class is in parentheses. Results were corrected with *18S* expression values and are presented as relative values to that of A549, which was given a value of 1. Bars, SD. *, $P < 0.05$; **, $P < 0.01$, *t*-test. C, Western blotting analyses of POLD4 and POLD1 were carried out using a panel of lung cancer cell lines. D, the 149 NSCLC patients were classified into two groups according to *POLD4* expression level, with the threshold set at −1 SD of the average. Kaplan-Meier survival curves for these groups showed a significant difference in both overall and relapse-free survival. *P* values were determined using a log-rank test.

48 hours. Viable cells were measured in triplicate using TetraColor One (Seikagaku) with reference to the viability of mock-treated cells.

Cell cycle synchronization

Calu6 was synchronized according to the method of Nakagawa et al. (8), with some modifications. Briefly, 24-hour treatment with 2 mmol/L thymidine was used to arrest exponentially proliferating cells in the S phase. The cells were then released from arrest by three washes in PBS, then si*CTRL*- and si*D4*-treated cells were grown in fresh medium for 12 and 15 hours, respectively. The release times were not the same due to a delayed cell cycle progression by si*D4*. Aphidicolin at 1 μmol/L was used for the second block for 24 hours, then the cells were released by three washes in PBS, incubated in normal culture medium for various times, and harvested for flow-cytometric and Western blotting analyses.

Chromosomal analysis

Colcemid at 0.1 μg/mL was added to the culture medium for 2 hours, then HCT116 cells were harvested, washed with PBS, and incubated at 37°C in 75 mmol/L KCl for 30 minutes, followed by centrifugation at 1,500 rpm for 5 minutes. The cells were further incubated in Carnoy's solution (methanol: acetate = 3:1) for 30 minutes, collected by centrifugation at 800 rpm for 5 minutes, resuspended in 0.5 mL of Carnoy's solution, dropped onto a wet (75% ethanol) slide glass from a height of 30 cm, and flamed with a burner. The slide glass

Published OnlineFirst September 22, 2010; DOI:10.1158/0008-5472.CAN-10-0784

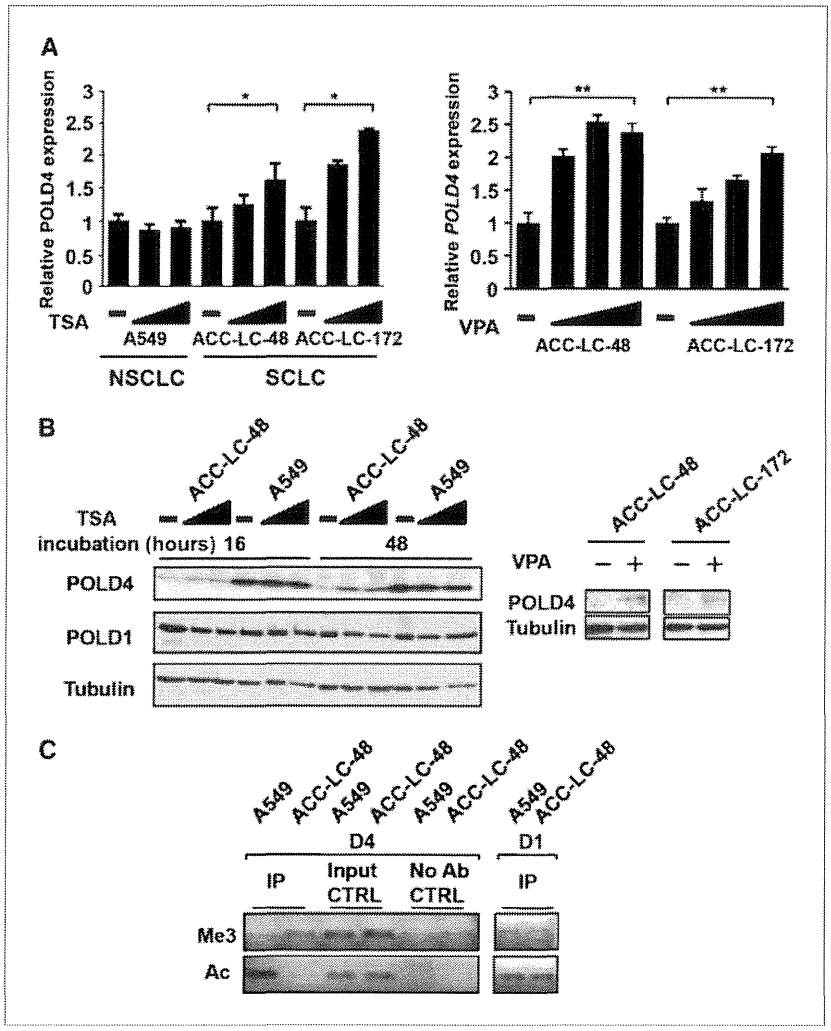

Figure 2. Detection of histone modifications. A, after treating cells with 0, 0.25, or 1 μg/mL of trichostatin A (TSA) for 48 (A549 and ACC-LC-48) or 16 (ACC-LC-172) hours (left), or with 0, 0.5, 1, or 2 μmol/L of valproic acid (VPA) for 16 hours (right), total RNA was extracted and quantitative RT-PCR was performed. The results were corrected by *18S* expression values and are presented as relative to that without drugs, which was set at 1. Bars, SD. *, $P < 0.05$; **, $P < 0.01$, *t*-test. B, ACC-LC-48 and A549 cells were treated with 0, 0.25, or 1 μg/mL of TSA for 16 or 48 hours, then Western blotting analysis was performed for detection of POLD4 and POLD1, with α-tubulin used as the control (left). Western blotting analysis was also performed for POLD4 with or without 2 mmol/L VPA. C, chromatin immunoprecipitation samples were prepared as described in Materials and Methods. Input controls represent samples not subjected to immunoprecipitation (IP). In the promoter region of *POLD4* of the NSCLC cell line A549, histone H3 was acetylated at a level 5.6 ± 2.4-fold greater as compared with the SCLC cell line ACC-LC-48. The trimethylation level of Lys9 of histone H3 in ACC-LC-48 was 3.6 ± 2.2-fold greater than that in A549. In a control experiment to analyze histone H3 modifications in the *POLD1* promoter, similar amounts of acetylation and methylation were detected in the two cell lines.

was left overnight at room temperature, then dipped into 4% Giemsa solution for 15 minutes, rinsed with water from the opposite side of the sample, air-dried, and shielded by a coverslip. Mitotic chromosomes were analyzed using a Bx 60 microscope (Olympus), and the Invision V 4.07 (Biovision Technology) and Photoshop (Adobe) software packages.

Results

Low expression of *POLD4* mRNA and POLD4 protein in SCLC

Genomic instability is thought to underlie the pathogenesis of lung cancer. To elucidate the underlying mechanisms, we screened for genes involved in DNA metabolism (Dataset S1) using our previous profiling data set consisting of 149 cases of NSCLC, 9 cases of SCLC, and 5 normal lung mixture specimens (14). We found that *POLD4* expression was distinctly reduced in SCLC, whereas a small fraction of NSCLC specimens also had a low expression of *POLD4* that was comparable with SCLC (Fig. 1A). In contrast, other DNA pol δ subunits had expression levels in the order of SCLC > NSCLC > normal lung (Fig. 1A), whereas the majority of growth-related mRNAs had increased levels of expression in the lung cancer specimens (Supplementary Fig. S1A). In hierarchical clustering analysis, *POLD4* was found in a distant small branch (Supplementary Fig. S2), suggesting a unique control mechanism of *POLD4* expression. RT-PCR findings from a second panel of clinical samples confirmed our results (Fig. 1B). In addition, distinctive downregulation of *POLD4* was observed in another database set (Supplementary Fig. S1B).

The low level of *POLD4* expression seen is unlikely attributable to the detection of splicing variants (Supplementary Fig. S3).Western blotting analysis showed that POLD4 (alternatively called p12) was detected at the level of the background in ACC-LC-76 and -172 (Fig. 1C). In addition, two other SCLC cell lines showed marginal expression levels, whereas apparent expressions were also observed in the NSCLC cell lines. In contrast, both panels of cell lines expressed a comparable amount of POLD1 (p125). It was also noted that a fraction of NSCLC specimens with low POLD4

Published OnlineFirst September 22, 2010; DOI:10.1158/0008-5472.CAN-10-0784

expression levels comparable with SCLC were associated with poor prognosis (Fig. 1D). In accord with the low level of mRNA expression (Supplementary Fig. S4), *POLD4* was induced by trichostatin A or valproic acid, class I and II mammalian histone deacetylase inhibitors, in ACC-LC-48 and -172 (Fig. 2A and B). ACC-LC-48 was further shown to be associated with higher histone H3K9 methylation and lower acetylation patterns in the *POLD4* promoter region than was A549 (Fig. 2C). *POLD4* expression in ACC-LC-76 was induced by 5 aza-2' deoxycytidine, although the promoter methylations were not dense and their contribution to *POLD4* expression is yet to be studied (Supplementary Fig. S5A). On the other hand, proteasome-dependent protein degradation pathways did not seem to play a major role (Supplementary Fig. S5B).

POLD4-deficient pol δ impairs pol and nucleotide excision DNA repair activities

Because pol δ is an essential protein complex for DNA replication and repair (15, 16), a subunit stoichiometry of the pol δ complex is required to exclude the possibility that POLD4 expression in SCLC and a fraction of NSCLC is sufficient for constituting the 4-subunit structure of the pol δ complex. POLD4 was identified in the immunoprecipitated pol δ complex using the anti-POLD1 antibody in the A549 cell line with a high expression of POLD4, but not in ACC-LC-172 cells with a low level of POLD4 (Fig. 3A), which strongly suggests that most of pol δ in ACC-LC-172 cells lack POLD4. In the presence of pol δ accessory proteins, including PCNA, RPA, and RFC, POLD4-deficient pol δ showed DNA replication activity that was lower than that of intact pol δ (Fig. 3B and C), which supports a previous finding (17, 18). We also examined the functional consequences of reduced POLD4 expression in lung cancer pathogenesis. To this end, we attempted to establish SCLC cell lines with ectopic POLD4 expression, although most of the SCLC cells did not allow POLD4 overexpression (data not shown); such intolerance has also been reported for another replicative DNA polymerase subunit, POLA1 (19). For this reason, we chose the NSCLC cell line

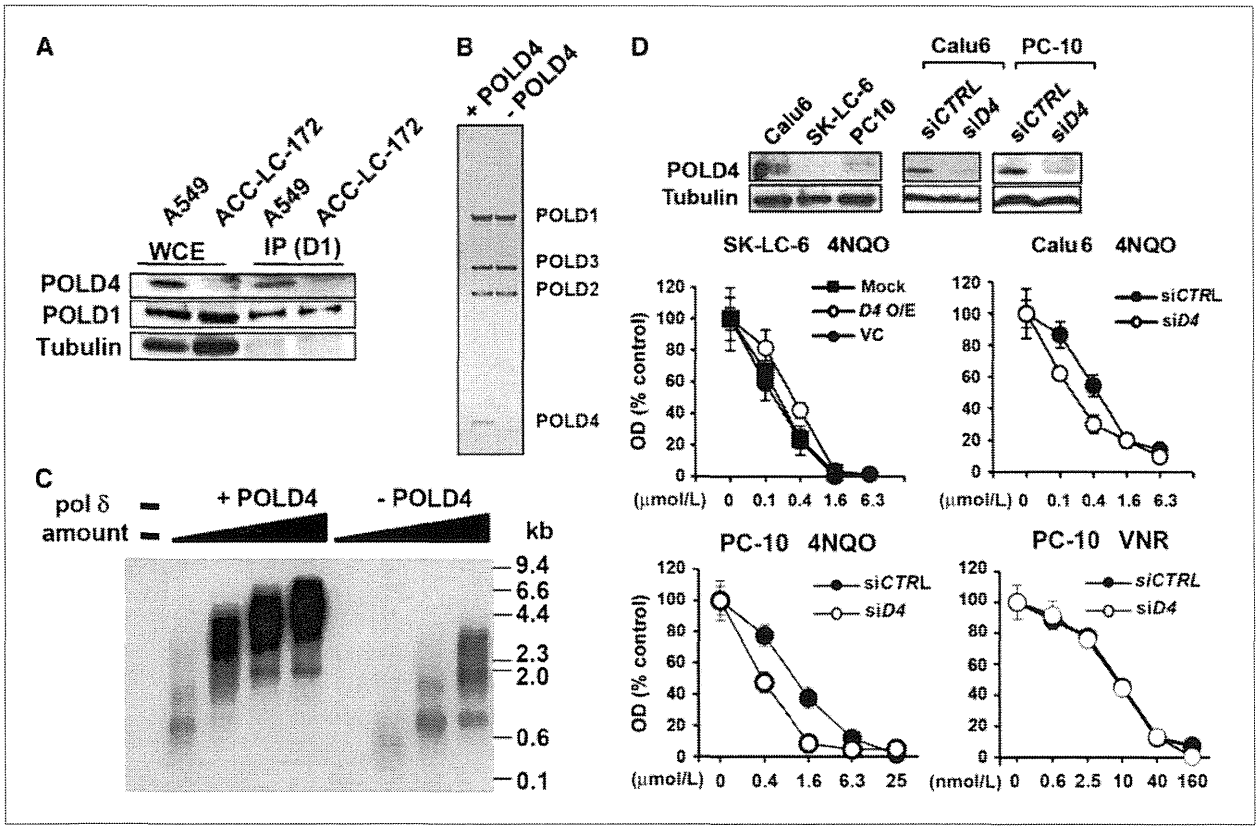

Figure 3. Effects of POLD4 depletion on *in vitro* pol δ and NER activities. A, after immunoprecipitation was performed using the anti-POLD1 antibody (IP), POLD4 and POLD1 were detected by Western blotting analysis. A whole cell extract (WCE) was used as the control. B, the purity of the recombinant pol δ complex with or without the POLD4 subunit was analyzed by SDS gel electrophoresis. Each subunit is indicated on the right. C, DNA replication activity between the two structures of pol δ was compared in the presence of accessory proteins using primed M13 DNA as a template primer. The length of the synthesized DNA is indicated on the right. The amounts of pol δ complexes in the reactions varied from 0 to 88 ng, as described in Materials and Methods. D, expression levels of POLD4 in Calu6, SK-LC-6, and PC-10 cells. Depletion of POLD4 was monitored in Calu6 and PC-10 cells treated with either si*CTRL* or si*D4*. Below, results of MTT assays to determine cell growth two days after treatment with various concentrations of drugs. OD values with no drug were regarded as 100%. Clones and siRNA treatments are indicated. *D4O/E* and VC represent clones with POLD4 overexpression and the vector control, respectively.

Published OnlineFirst September 22, 2010; DOI:10.1158/0008-5472.CAN-10-0784

SK-LC-6, which has a low level of POLD4 expression. Although 4NQO produces a DNA adduct that is removed through pol δ–dependent nucleotide excision DNA repair (NER), POLD4-introduced SK-LC-6 cells were more resistant to 4NQO (Fig. 3D and Supplementary Fig. S6A). Similar results were obtained with the SCLC cell line ACC-LC-172, despite the findings that this cell line is intrinsically resistant to 4NQO (Supplementary Fig. S6B). In a reciprocal experiment using the NSCLC cell lines Calu6 and PC-10, siRNA treatment against *POLD4* (si*D4*) reduced the protein level to nearly one third of the original level, which resulted in increased sensitivity to 4NQO (Fig. 3D).

To examine whether POLD4 expression has any specificity to the NER pathway, the effects of POLD4 expression on sensitivities to vinorelbine, a microtubule assembly inhibitor, were studied. For this experiment, we used PC-10 cells, as they have modest sensitivity to a variety of drugs, indicating that this cell line has a low possibility of having abnormal drug metabolic pathways (data not shown). Our results showed that si*D4* did not alter the sensitivity to vinorelbine (Fig. 3D).

POLD4 required for cell cycle progression

A previous study showed that the *POLD4* ortholog of *Cdm1* in *Schizosaccharomyces pombe* (*S. pombe*) is a nonessential gene (20), although it may be required in mammalian cells (21, 22). To study human POLD4 functions, we depleted POLD4 using si*D4* and analyzed the cell cycle progression. In the NSCLC cell line Calu6 as well as in others, si*D4* altered the cell cycle of each population (Supplementary Fig. S7A and B), and induced p21 and p27 (Supplementary Fig. S7C).

We synchronized and released cells from the G_1-S boundary, and chased them. A fraction of the si*D4*-treated cells did not progress into the S-phase, but rather stayed at G_1-S (Fig. 4A, filled arrows). Again, persistent induction of p21 and p27 was detected (Fig. 4B). It was also observed that the timing of entry into the G_1 phase was not the same between si*CTRL* and si*D4* cells. In the latter, G_1 entry was seen 12 hours after release, which was 2 hours later than that with the si*CTRL* cells (Fig. 4A, open arrows). In addition, the DNA damage checkpoint genes NBS1, ATM, CHK2, SMC1, and CHK1 were phosphorylated throughout S to G_2 (Fig. 4C), suggesting that the cell cycle was delayed by activation of these checkpoint proteins. These phenotypes were rescued in stable clones that carried *pold4* with silent mutations at the si*D4* target site (Fig. 5). Additional knockdown of p27 resulted in efficient S-phase entry, which indicates that p27 induction inhibits cell cycle progression at the G_1-S boundary in Calu6 cells (Supplementary Fig. S8A–D).

These results suggest that POLD4 downregulation activates checkpoint proteins, induces G_1-S arrest, and delays the cell cycle from S to G_2. Generation of double-stranded DNA breaks (DSB) was also assessed by a knockdown experiment of DNAPK, a nonhomologous end-joining kinase, which had a synergistic effect with si*D4* on the G_1-S population (Supplementary Fig. S8E and F).

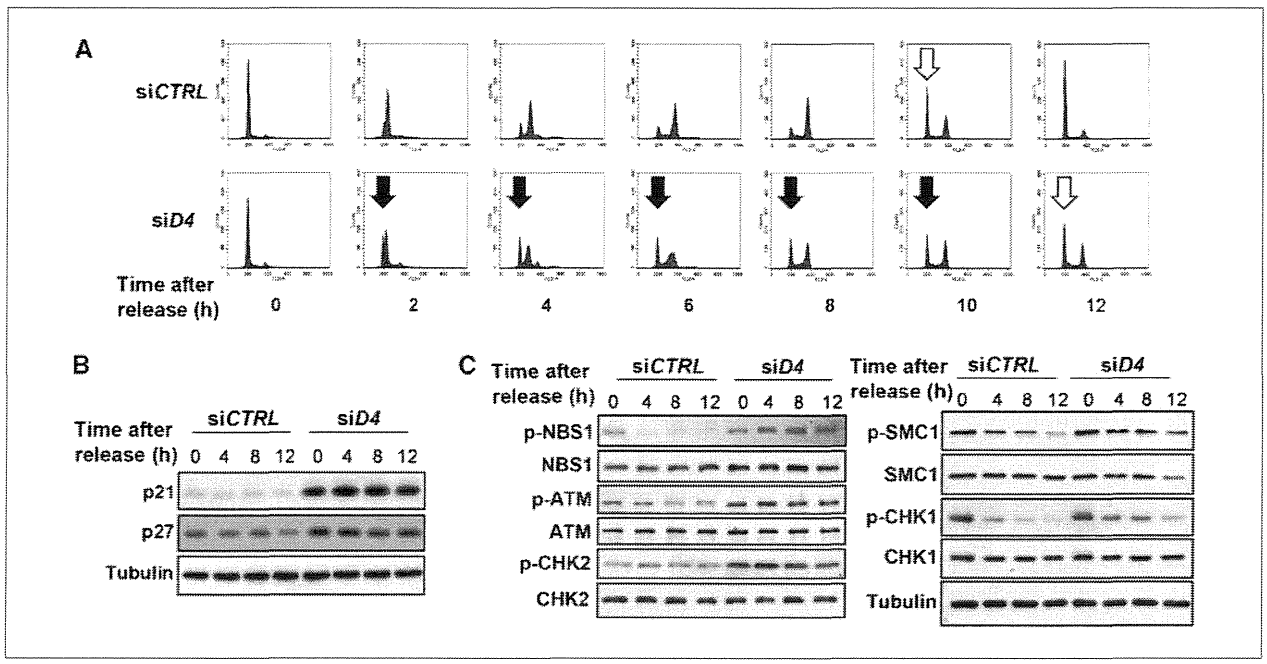

Figure 4. POLD4 reduction induces checkpoint activation. A, Calu6 cells were synchronized at the G_1-S boundary and released, then DNA contents were measured every two hours. Filled arrows, G_1-S arrested population; open arrows, G_1 re-entry. B, after treating Calu6 cells with siRNA for 48 hours, the cells were analyzed for the expression levels of G_1-S checkpoint proteins. C, at each time point after release, Western blotting analysis was performed using the indicated antibodies.

Published OnlineFirst September 22, 2010; DOI:10.1158/0008-5472.CAN-10-0784

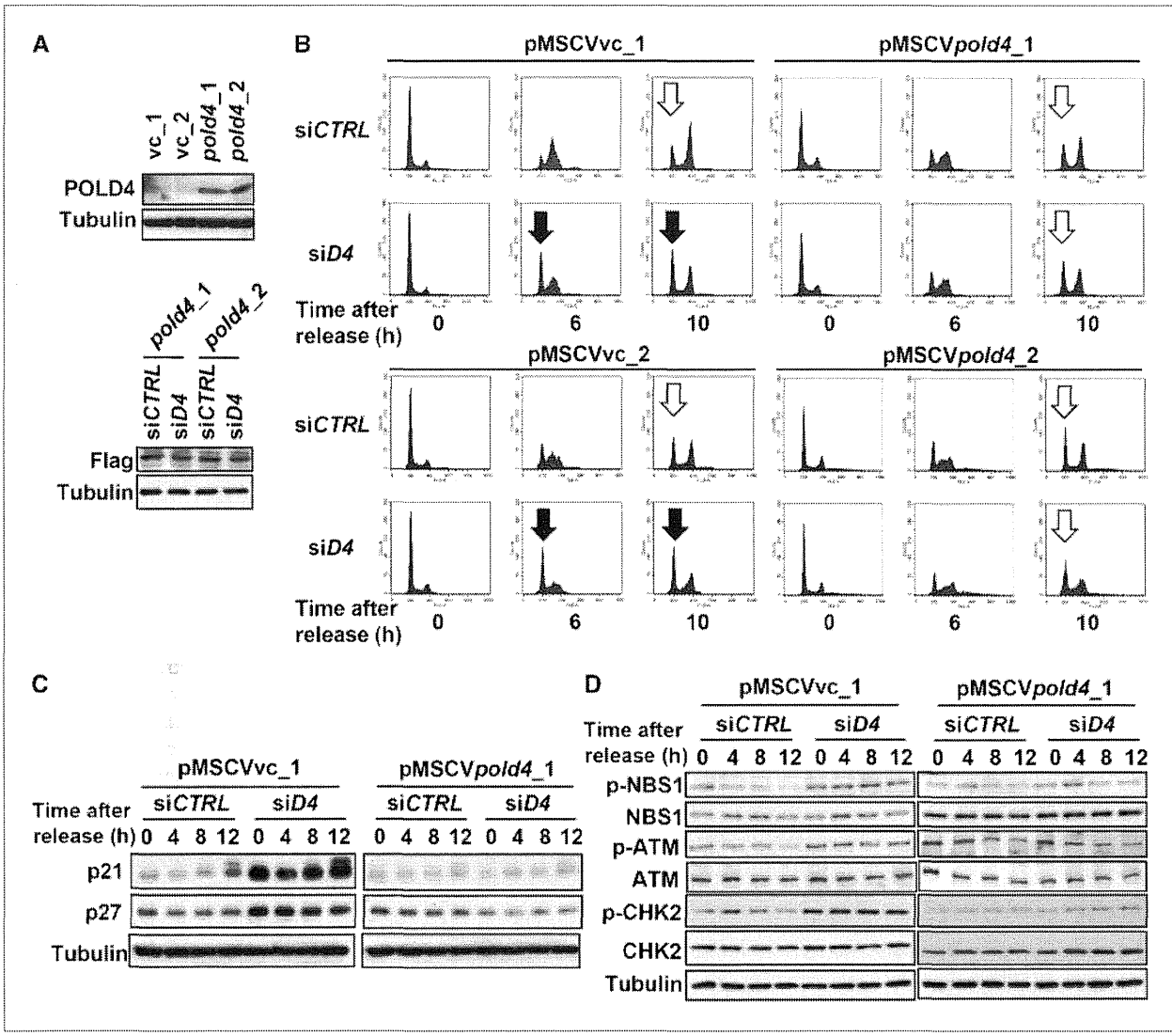

Figure 5. Ectopic overexpression of *POLD4* with silent mutations rescues cell cycle phenotypes. A, Western blotting analysis using the rabbit polyclonal anti-POLD4 antibody was carried out to monitor overexpression in Calu6 *pold4*_1 and _2 clones (top), which were resistant to si*D4* treatment (anti-FLAG antibody, bottom). B, Calu6 *pold4*_1 and _2 and the vector control clones of pMSCVvc_1 and _2 were synchronized and released, then monitored for DNA content. Filled arrows, G_1-S arrested population; open arrows, G_1 re-entry. C and D, at each time point after release, Western blotting analysis was performed using the indicated antibodies and Calu6 stable clones.

Induction of chromosome breaks and gaps by POLD4 reduction

Activation of the ATM, ATR, and DNA-PK pathways suggests that both DSB and single-stranded breaks were generated by POLD4 reduction. These results are in accord with our recent observation that SCLC cells are associated with constitutive DSB (5). Notably, POLD4 overexpression reduced the γ-H2AX intensity (Fig. 6A and B). Furthermore, we investigated whether POLD4 reduction also induces any chromosome aberrations. For this experiment, most lung cancer cell lines were not applicable to this particular purpose because they exhibit aneuploidy in association with chromosomal instability (23). We used HCT116 cells where POLD4 expression levels were sufficiently high (Fig. 6A). si*D4* treatment significantly increased the numbers of chromosomal gaps and breaks to twice as many as observed with si*CTRL* treatment, whereas this phenotype was readily suppressed in cells expressing *pold4* with silent mutations at the siRNA target site (Fig. 6A, C, and D).

Discussion

To date, despite the premise that deficits in DNA replication machinery account for multiple mutations in cancer (10), and findings showing that laboratory-born animals and strains defective in DNA replication machineries exhibit genomic instability (24, 25), core DNA replication proteins have rarely been identified as a frequent target for alterations

Published OnlineFirst September 22, 2010; DOI:10.1158/0008-5472.CAN-10-0784

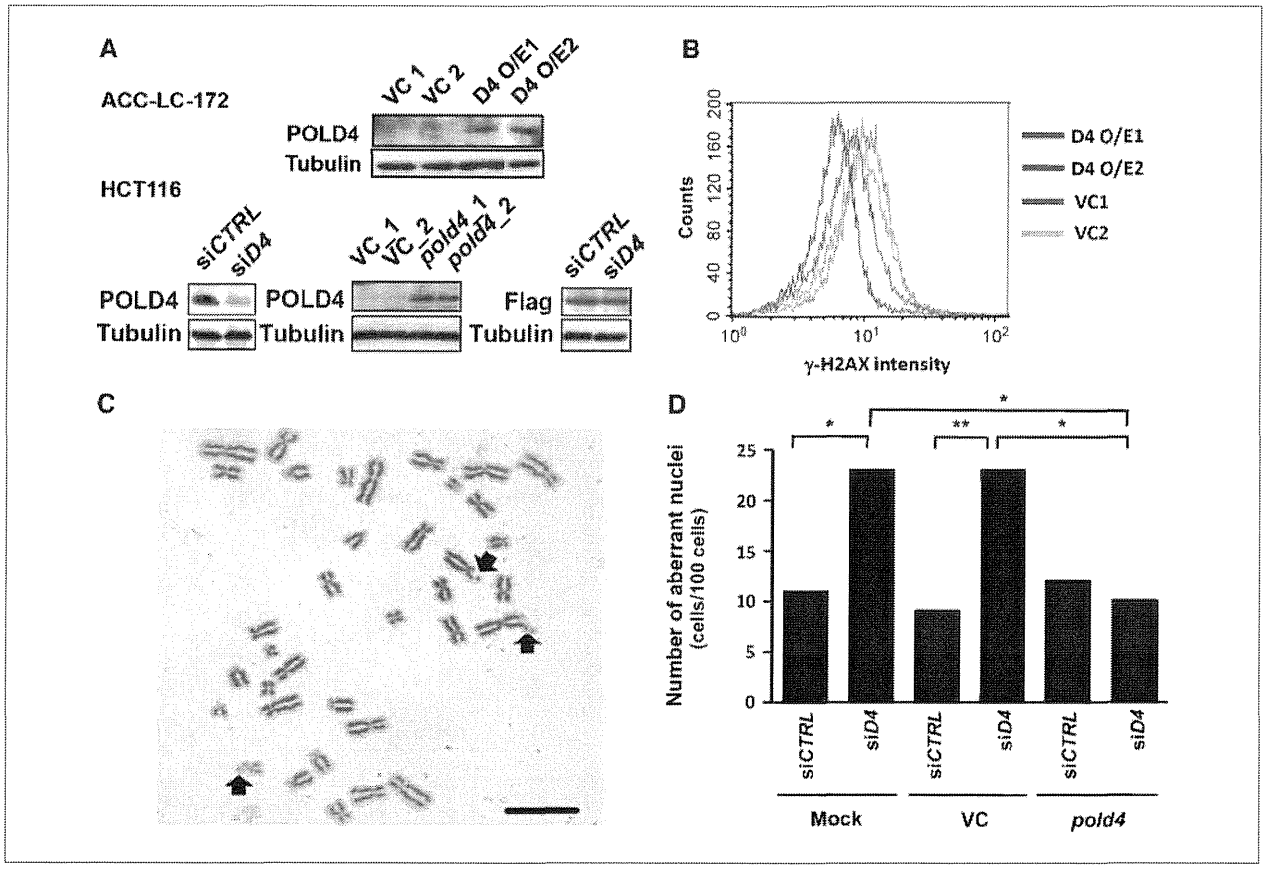

Figure 6. Chromosomal gap/break formation in cells. A, Western blotting analysis was performed to confirm the overexpression of POLD4 in the stable clones (ACC-LC-172, D4 O/E1, and O/E2). Shown are representative results of Western blotting analysis using HCT116 and the monoclonal antibody (left), HCT116 stable clones and the rabbit polyclonal anti-POLD4 antibody (middle), and a mixture of 7 stable clones with *pold4* overexpression and the anti-FLAG antibody (right), which were used to monitor silencing efficiency, overexpression, and resistance against si*D4* treatment, respectively. B, S-phase cells from ACC-LC-172 D4 O/E and control clones were quantitated in regard to γ–H2AX induction, as indicated. C, representative photograph of mitotic chromosomes. Arrows, chromosomal breaks; bar, 10 μmol/L. D, chromosomal gaps and breaks were quantitated by counting 100 mitotic cells. The numbers of cells with ≥2 gaps/breaks were plotted for mock, vector control (VC), and mD4-overexpressed HCT116 cells (*pold4*). Stable VC and mD4 clones were mixtures of 7 independent clones. *, $P < 0.05$; **, $P < 0.01$, Fisher's exact test). To acquire sufficient numbers of high-quality images, the sums of aberrations from five independent experiments were used for comparison. The numbers of total gaps/breaks are also shown in Supplementary Fig. S9.

in human cancers. The present results show that the pol δ subunit POLD4 is frequently reduced in some lung cancer specimens and cell lines, whereas overexpression of POLD4 complements part of the pathologic phenotypes of lung cancer cell lines.

It is interesting to note that although the POLD4 reduction was most evident in SCLC, which is a very aggressive form of lung cancer, a small fraction of NSCLC cases also showed low expression in association with poor prognosis. In *in vitro* experiments, we found that POLD4 is required to suppress DSB and subsequent checkpoint activation. Together with our previous findings that clinically obtained SCLC specimens were frequently associated with discrete γ-H2AX foci formation (5), these results suggest that reduced POLD4 expression may play a role in lung cancer progression in association with the genomic instability phenotypes.

Along this line, cells with impaired activity of replicative DNA polymerases induce deletions with short nucleotides (<1 kb) with similar base substitution spectra (26, 27), whereas the results of recent next-generation sequencing studies that utilized one sample each of SCLC and NSCLC showed frequent transversions in both types of cancer, and also indicated that SCLC carried significantly more frequent deletions (53 of 65) than NSCLC (93 of 424; $P = 1.28 \times 10^{-20}$, Fisher's exact test, denominators include all small insertions and deletions; refs. 28, 29). Impaired activity in replicative DNA polymerases is also known to increase the possibility of large deletions and duplications of chromosomes and arms (30, 31). Using datasets made from 74 lung adenocarcinoma patients for gene expression levels as well as copy number variations (32, 33), we noted that low *POLD4* expression was significantly associated with 8p, 9q, and 13q deletions, and 5p, 7p, 8q, and 14q amplifications, which are shared by both NSCLC and SCLC (refs. 34, 35; Supplementary Table S2). In addition, we observed that low *POLD4* expression in primary tumors was associated with high expression of *HDAC2* ($P = 0.0036$; see

Published OnlineFirst September 22, 2010; DOI:10.1158/0008-5472.CAN-10-0784

Supplementary Information), which was in accord with our *in vitro* data showing that *POLD4* expression is regulated by histone modifications.

SCLC exhibits aggressive cell growth leading to very poor clinical prognosis, although it is also characterized by large areas of necrosis (36) and cell lines are difficult to establish (37). The putative growth disadvantage due to low POLD4 might be partially compromised by the characteristics of SCLC. First, G_1-S transition may be supplemented by factors that are highly expressed in SCLC. With regard to this speculation, it has been reported that *CDC6* and *CDT1*, which are recruited at G_1-S for licensing the DNA replication, are abnormally overexpressed in the early stage of carcinogenesis (38). In our analysis of SCLC, >10-fold expressions of *CDC6* and *CDT1* were observed in the specimens (Supplementary Fig. S1A). The G_1-S transition may be thereby facilitated by forced entry into the S phase in SCLC. Second, nearly all SCLC tumors are deficient of Rb and p53, which are critical regulators for G_1-S transition (1, 23). Checkpoint impairment may benefit SCLC cell proliferation, survival, increased genomic instability, and tumor progression, as well as suppress the growth defect induction caused by POLD4 downregulation. Third, the *POLD4* ortholog of *Cdm1* is a nonessential gene in *S. pombe* (20). Although the complexity of the DNA replication mechanisms and amounts of chromosomal DNA are not the same between yeast and human cells, si*D4*-treated cells were able to proliferate throughout the cell cycle, as shown in Fig. 4 (22).

Tobacco smoke contains benzo(a)pyrene, one of the most potent carcinogens, whereas DNA adducts of benzo(a)pyrene are removed by pol δ–dependent NER as are those of 4NQO. Along this line, previous epidemiologic studies have indicated a strong association of lung cancer with tobacco smoking (1). Benzo(a)pyrene adducts might remain in DNA and drive genomic instability in lung cells with reduced POLD4 expression. This notion is also in line with a recent hypothesis that DNA replication stress leads to DSB, genomic instability, and selective pressure for later p53 mutations (3, 5, 6). It is important to note, however, that involvement of POLD4 as a crucial effecter of an unidentified primary target for genetic/epigenetic alterations in lung cancer cannot be formerly precluded. Future studies, such as with genetically engineered mice, are required to determine whether POLD4 downregulation is involved in the early stage of carcinogenesis or if it contributes to the late progression stage.

Our results indicate that POLD4 is required for maintenance of genomic stability of human cells. With low expression levels of POLD4, lung cancer may grow with accumulation of DNA damage. Publicly available datasets show that *POLD4* expression levels vary widely in other types of cancer, although most datasets do not contain information for corresponding normal tissues. It would be interesting to study whether POLD4 reduction is specific to lung cancer or may be involved in the development of other types of cancer.

Disclosure of Potential Conflicts of Interest

No potential conflicts of interest were disclosed.

Grant Support

A Grant-in-Aid for Scientific Research on Innovative Areas, a Grant-in-Aid for Scientific Research on Priority Areas from the Ministry of Education, Culture, Sports, Science, and Technology of Japan, a Grant-in-Aid for Scientific Research from the Japan Society for the Promotion of Science, and the Personalized Medicine Project of the Japan Science and Technology Agency.

The costs of publication of this article were defrayed in part by the payment of page charges. This article must therefore be hereby marked *advertisement* in accordance with 18 U.S.C. Section 1734 solely to indicate this fact.

Received 03/05/2010; revised 08/23/2010; accepted 09/07/2010; published OnlineFirst 09/22/2010.

References

1. Osada H, Takahashi T. Genetic alterations of multiple tumor suppressors and oncogenes in the carcinogenesis and progression of lung cancer. Oncogene 2002;21:7421–34.
2. Worden FP, Kalemkerian GP. Therapeutic advances in small cell lung cancer. Expert Opin Investig Drugs 2000;9:565–79.
3. Bartkova J, Horejsi Z, Koed K, et al. DNA damage response as a candidate anti-cancer barrier in early human tumorigenesis. Nature 2005;434:864–70.
4. Ebi H, Matsuo K, Sugito N, et al. Novel NBS1 heterozygous germ line mutation causing MRE11-binding domain loss predisposes to common types of cancer. Cancer Res 2007;67:11158–65.
5. Ebi H, Sato T, Sugito N, et al. Counterbalance between RB inactivation and miR-17–92 overexpression in reactive oxygen species and DNA damage induction in lung cancers. Oncogene 2009;28:3371–9.
6. Gorgoulis VG, Vassiliou LV, Karakaidos P, et al. Activation of the DNA damage checkpoint and genomic instability in human precancerous lesions. Nature 2005;434:907–13.
7. Konishi H, Nakagawa T, Harano T, et al. Identification of frequent G(2) checkpoint impairment and a homozygous deletion of 14–3-3ε at 17p13.3 in small cell lung cancers. Cancer Res 2002;62:271–6.
8. Nakagawa T, Hayashita Y, Maeno K, et al. Identification of decatenation G2 checkpoint impairment independently of DNA damage G2 checkpoint in human lung cancer cell lines. Cancer Res 2004;64:4826–32.
9. Kaufmann WK. Initiating the uninitiated: replication of damaged DNA and carcinogenesis. Cell Cycle 2007;6:1460–7.
10. Bielas JH, Loeb LA. Mutator phenotype in cancer: timing and perspectives. Environ Mol Mutagen 2005;45:206–13.
11. Osada H, Tatematsu Y, Masuda A, et al. Heterogeneous transforming growth factor (TGF)-β unresponsiveness and loss of TGF-β receptor type II expression caused by histone deacetylation in lung cancer cell lines. Cancer Res 2001;61:8331–9.
12. Osada H, Tatematsu Y, Sugito N, Horio Y, Takahashi T. Histone modification in the TGFβRII gene promoter and its significance for responsiveness to HDAC inhibitor in lung cancer cell lines. Mol Carcinog 2005;44:233–41.
13. Masuda Y, Suzuki M, Piao J, Gu Y, Tsurimoto T, Kamiya K. Dynamics of human replication factors in the elongation phase of DNA replication. Nucleic Acids Res 2007;35:6904–16.
14. Takeuchi T, Tomida S, Yatabe Y, et al. Expression profile-defined classification of lung adenocarcinoma shows close relationship with underlying major genetic changes and clinicopathologic behaviors. J Clin Oncol 2006;24:1679–88.
15. Pavlov YI, Frahm C, McElhinny SA, Niimi A, Suzuki M, Kunkel TA. Evidence that errors made by DNA polymerase α are corrected by DNA polymerase δ. Curr Biol 2006;16:202–7.
16. Pavlov YI, Shcherbakova PV, Rogozin IB. Roles of DNA polymerases in replication, repair, and recombination in eukaryotes. Int Rev Cytol 2006;255:41–132.
17. Li H, Xie B, Zhou Y, et al. Functional roles of p12, the fourth subunit of human DNA polymerase δ. J Biol Chem 2006;281:14748–55.